2014

LATE QUATERNARY CRUSTAL DEFORMATION AT THE APEX OF THE MOUNT MCKINLEY RESTRAINING BEND OF THE DENALI FAULT, ALASKA

Corey A. Burkett
University of Kentucky, coreyburkett@gmail.com

STUDENT AGREEMENT:

I represent that my thesis or dissertation and abstract are my original work. Proper attribution has been given to all outside sources. I understand that I am solely responsible for obtaining any needed copyright permissions. I have obtained needed written permission statement(s) from the owner(s) of each third-party copyrighted matter to be included in my work, allowing electronic distribution (if such use is not permitted by the fair use doctrine) which will be submitted to UKnowledge as Additional File.

I hereby grant to The University of Kentucky and its agents the irrevocable, non-exclusive, and royalty-free license to archive and make accessible my work in whole or in part in all forms of media, now or hereafter known. I agree that the document mentioned above may be made available immediately for worldwide access unless an embargo applies.

I retain all other ownership rights to the copyright of my work. I also retain the right to use in future works (such as articles or books) all or part of my work. I understand that I am free to register the copyright to my work.

REVIEW, APPROVAL AND ACCEPTANCE

The document mentioned above has been reviewed and accepted by the student's advisor, on behalf of the advisory committee, and by the Director of Graduate Studies (DGS), on behalf of the program; we verify that this is the final, approved version of the student's thesis including all changes required by the advisory committee. The undersigned agree to abide by the statements above.

Corey A. Burkett, Student

Dr. Sean P. Bemis, Major Professor

Dr. Edward W. Woolery, Director of Graduate Studies

LATE QUATERNARY CRUSTAL DEFORMATION AT THE APEX OF THE MOUNT MCKINLEY RESTRAINING BEND OF THE DENALI FAULT, ALASKA

THESIS

A thesis submitted in partial fulfillment of the requirements for the degree of Master of Science in the College of Arts and Sciences at the University of Kentucky

By
Corey Austin Burkett
Lexington, Kentucky

Director:
Dr. Sean P. Bemis, Assistant Professor of Earth and Environmental Sciences
Lexington, Kentucky
2014

ABSTRACT OF THESIS

LATE QUATERNARY CRUSTAL DEFORMATION AT THE APEX OF THE MOUNT MCKINLEY RESTRAINING BEND OF THE DENALI FAULT, ALASKA

The tallest mountain in North America, Mount McKinley is situated inside a sharp bend in the right-lateral Denali fault. This anomalous topography is clearly associated with the complex geometry of the Denali fault, but how this topography evolves in conjunction with the adjacent strike-slip fault is unknown. To constrain how this fault bend is deforming, the Quaternary fault-related deformation on the opposite side of the Denali fault from Mount McKinley were documented through combined geologic mapping, active fault characterization, and analysis of background seismicity. My mapping illustrates an east-west change in faulting style where normal faults occur east of the fault bend and thrust faults predominate to the west. These faults offset glacial outwash terraces and moraines which, with tentative correlations with the regional glacial history, provide fault slip rates that suggest that the Denali fault bend is migrating southwestward. The complex and elevated regional seismicity corroborates the style of faulting associated with the fault bend and provide additional subsurface control on the location of active faults. Seismologic and neotectonic constraints suggest that the maximum compressive stress axis rotates from vertical east of the bend to horizontal and Denali fault-normal west of the bend.

KEYWORDS: Active Tectonics, Restraining Bends, Denali Fault, Surficial Mapping

Corey Austin Burkett

December 18, 2014

QUATERNARY CRUSTAL DEFORMATION AT THE APEX OF THE MOUNT MCKINLEY RESTRAINING BEND OF THE DENALI FAULT, ALASKA

By

Corey Austin Burkett

Dr. Sean Bemis

Director of Thesis

Dr. Edward W. Woolery

Director of Graduate Studies

December 18, 2014

ACKNOWLEDGMENTS

This thesis benefitted from the guidance, inspiration, and support of many individuals and organizations. I would like to gratefully acknowledge the direction, expertise and encouragement of my advisor, Dr. Sean Bemis. Thank you for encouraging my research and for allowing me to grow as a research scientist.

I would also like to acknowledge Dr. Ed Woolery, and Dr. Zhenming Wang for their help as committee members throughout this thesis process. I am sincerely grateful to them for their inspiring guidance, invaluably constructive criticism and friendly advice during this journey. In addition, a special thank you to Dr. Woolery, who made my time at the University of Kentucky very memorable. I will always cherish our conversions in the Seismic Lab, and I am grateful for the friendship that will continue into the future. I also want you to know that my wife's bake goods are only a shipment away.

During my two years spent at the University of Kentucky, my research in the Alaska Range has also benefited greatly from the ideas, support, and encouragement of my following colleagues (in addition to the individuals mentioned above): Dr. Jeff Benowitz, Dr. Julie Elliott, Dr. Brent Goehring, Clayton Brengman, Alice Orton, Stephen Prosser, and Patrick Terhune.

Outside of the scholarly realm, I received constant support from my friends and family. To all of my friends who supported me in writing and pushed me to strive towards my goals, thank you. To my family, a special thank you is needed because words cannot express how grateful I am to my siblings, in-laws, and parents for all of the sacrifices that you have made on my behalf. Lastly, I would like to express appreciation to my beloved wife, Audrey, who was willing, at all times, to lend a helping hand, a listening ear and a comforting smile.

Significant funding for this research was provided by as a part of the National Science Foundation – Tectonics funded project titled: Collaborative Research: A late Cenozoic record of restraining bend initiation and evolution along the Denali fault at Mount McKinley, Alaska (EAR – 1250461). My sincere thanks are also extended for the generous financial assistance provided by the Graduate School and the Department of Earth & Environmental Sciences at the University of Kentucky.

TABLE OF CONTENTS

LIST OF TABLES

LIST OF FIGURES

CHAPTER ONE: INTRODUCTION

1.1 Background

Strike slip faults are complex systems that commonly have geometric anomalies resulting in local zones of convergence or divergence. Restraining bends are those anomalies that accommodate convergence, forming zones of localized transpression (Cunningham and Mann, 2007). Their formation is a result of curvature along a strike-slip fault which creates space problems between fault blocks (Crowell, 1974). This forces shortening and vertical displacement of crustal material in order to allow for continued lateral movement (Legg et al., 2007) and to improve the mechanical efficiency of the strike-slip fault (Cooke et al, 2013). The transpression of a restraining bend can vary from a system that partitions slip into pure strike-slip and pure dip-slip faults to an area dominated by oblique-slip faults. A better understanding of how a bend forms and behaviors through time will be aided from drawing comparisons with similar classified systems. The classification of restraining bends defines a systematic relationship between the structure and deformation of the bend with its associated geometry.

In a global compilation of restraining and releasing bends, Mann (2007), separates restraining bends into 3 types: transpressional uplifts, sharp restraining bends, and gentle restraining bends (Figure 1.1). A transpressional uplift occurs along a generally straight segment of the major strike-slip fault where the block or plate motion is oblique to the master fault allowing simple and pure shear to occur together (e.g. Little, 1990). A sharp restraining bend has a rhomboidal shape and is characterized by a localized uplift on a fold and thrust belt. A gentle restraining bend

usually has a lazy S or Z shape and is characterized by its board deformation zone. The most common restraining bend type is the gentle restraining bend and includes some of the largest restraining bends in the world.

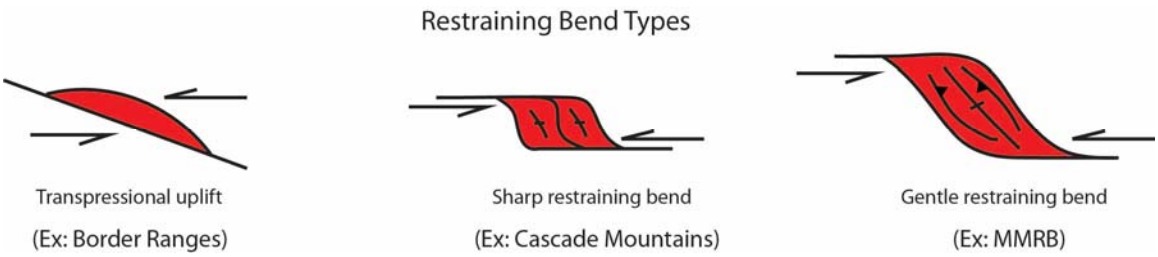

Figure 1.1: Restraining bend classification. Modified from Mann, (2007). Restraining bend classification of ancient and active restraining bends around the world. MMRB = Mt. McKinley restraining bend.

The Mount McKinley restraining bend in the Alaska Range is classified as a gentle restraining bend, and has led to the formation of the highest topographic peak of the mountain range and of North America, Mount McKinley. The Alaska Range is a major, active orogen formed along the arcuate, intracontinental, strike-slip Denali fault. This Alaska Range – Denali fault system is a far-field expression of the flat-slab subduction and the accretion processes associated with the Pacific-North America convergent plate boundary in southern Alaska (Figure 1.2) (Ferris et al., 2003; Eberhart-Phillips et al., 2006; Freymueller et al., 2008; Haeussler, 2008; Jadamec et al., 2013). The Alaska Range is the orogenic product of oblique plate motion (Sanderson and Marchini, 1984; Teyssier et al., 1995) imposed upon the Denali fault producing significant shortening expressed as parallel thrust faults to the north and

oblique thrust faults to the south of the fault (Figure 1.2). A prominent feature of the Denali fault is an abrupt 17 degree southwestward bend in the trace of the fault that defines the Mount McKinley restraining bend (MMRB). Significant shortening over millions of years inside the bend has made it possible for the formation of Mount McKinley.

Mount McKinley highlights the strongly asymmetric topography seen across the restraining bend. The south side of the Denali fault through the MMRB is dominated by a wide, broad swath of tall, rugged, glaciated peaks whereas the north side has a narrow band of foothills (the Peters Dome foothills) parallel to the Denali fault that broaden to the northwest (Figure 1.3). The topographic contrast across the MMRB suggests that the bend has a strong structural control on orogenic development. Despite the expectation for significant active deformation associated with restraining bends, only a couple Quaternary-active faults, the Peters Dome fault and the East Fork faults, were previously identified to the north of the Denali fault through the MMRB (Koehler et al., 2012). However, even first-order observations of regional seismicity, topographic data, and satellite imagery demonstrates the presence of an array of active structures that appear to be part of this transpressional system.

The MMRB exhibits a high level of background seismicity with M2 and larger earthquakes occurring weekly at depths less than 20 km (http://www.aeic.alaska.edu/). While relatively frequent, the historic earthquakes are small (<M3), with the cumulative seismic moment only equivalent to a moment magnitude of M5.6 during the time interval of 1990 to 2006 (Burris, 2006). Typically

referred to as the Kantishna Cluster (e.g. Ruppert et al., 2008) this seismologic phenomenon of high rate, clustered seismicity and suggests the occurrence of active Quaternary deformation in the Peters Dome foothills. Although, previous work has defined multiple seismic subzones in the Kantishna Cluster (Ruppert et al., 2008; Burris, 2007; Ratchkovski and Hansen, 2002), no geologic studies have not been conducted to identify the faults associated with this seismicity or to define the source of this seismicity. The cluster is located to the west of the eastern apex of the MMRB in line with the foothills propagating to the northwest with only some earthquakes occurring to the east of the apex. The abundance of earthquake events overlaying the foothills to the west of the eastern apex suggests a migration in the active deformation to the west with the lack of seismicity and active Quaternary surface deformation overlaying the foothills to the east of the apex. This suggests a long-term behavior of the restraining bend controlling deformation around the eastern apex.

The long-term behavior of restraining bend geometry has direct implications for how crustal material adverts through the restraining bend and the resulting exhumation, topographic development, and configuration of active faults. Some restraining bends geometrically appear to migrate along the trace of the primary strike-slip fault through time, such as those on the northern San Andreas fault of California (e.g. Wakabayashi, 2007). These bends in California produced low topography because the new transverse structures needed for migration continued to form in new crustal material and do not allow for the continuous uplift of crustal material (Wakabayashi, 2007). Alternatively, significant topographic highs or peaks along restraining bends, like the Mount McKinley, are typically associated with

restraining bends that are stationary or fixed along the trace of the primary fault, allowing for continuous uplift of crustal material (Cunningham and Mann, 2007). In the case of the MMRB, we have a major restraining bend containing an extreme topographic high with observations suggesting that the restraining bend is migrating. These characteristics are contrary to the general understanding of how restraining bends evolve suggesting that other factors are contributing to the unique behavior of the MMRB. Through a fundamental study of the Quaternary deformation to the north of the bend by establishing geologic controls on the Quaternary geology, the structural geology, and the seismicity, I present evidence for how the eastern apex of the MMRB is deforming and migrating that should help to isolate new constraints as to how this restraining bend maintains high topography and is associated with a migrating restraining bend.

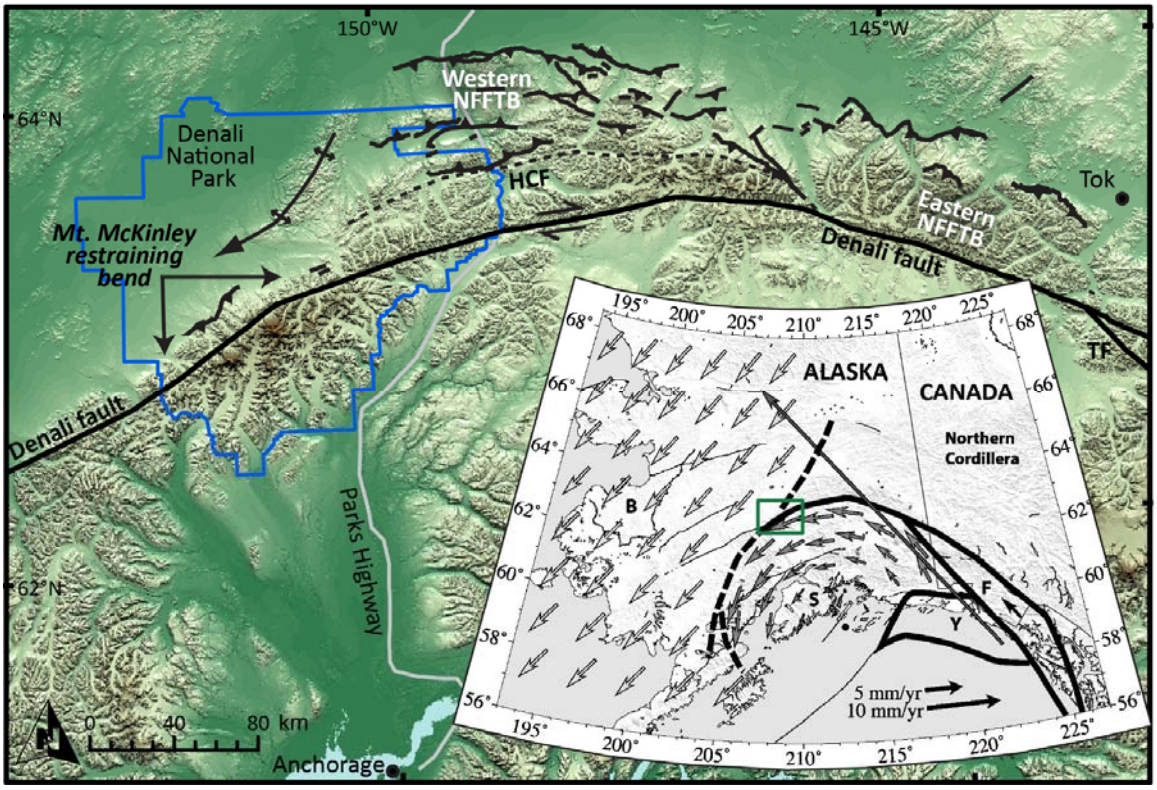

Figure 1.2: Simplified regional tectonic and topography of central Alaska. The inset map, from Freymueller et al. (2008), shows the movement of crustal blocks adjacent to the Denali fault relative to North America. The Yakutat block (Y) coupled with the Pacific plate is being subducted under the North America plate with a northwest convergence motion. The convergent boundary produces far-field strain represented by the Alaska Range and the counter-clockwise rotation of the Southern Alaska Block (S). While north of the Denali fault, the Bering Block (B) rotates clockwise. F = Fairweather Block. The green box on the inset depicts the Mount McKinley restraining bend (MMRB) seen in Figure 1.3. The arrows on the blocks are scaled for relative velocity with a key at the bottom. The main map shows the northern foothills of the Alaska Range west of the intersection of the Denali fault with the Totschunda fault (TF). The Kantishna Hills region is the westernmost element of the Alaska Range located inside Denali National Park, where there is substantial young topography to the north of the Denali fault.

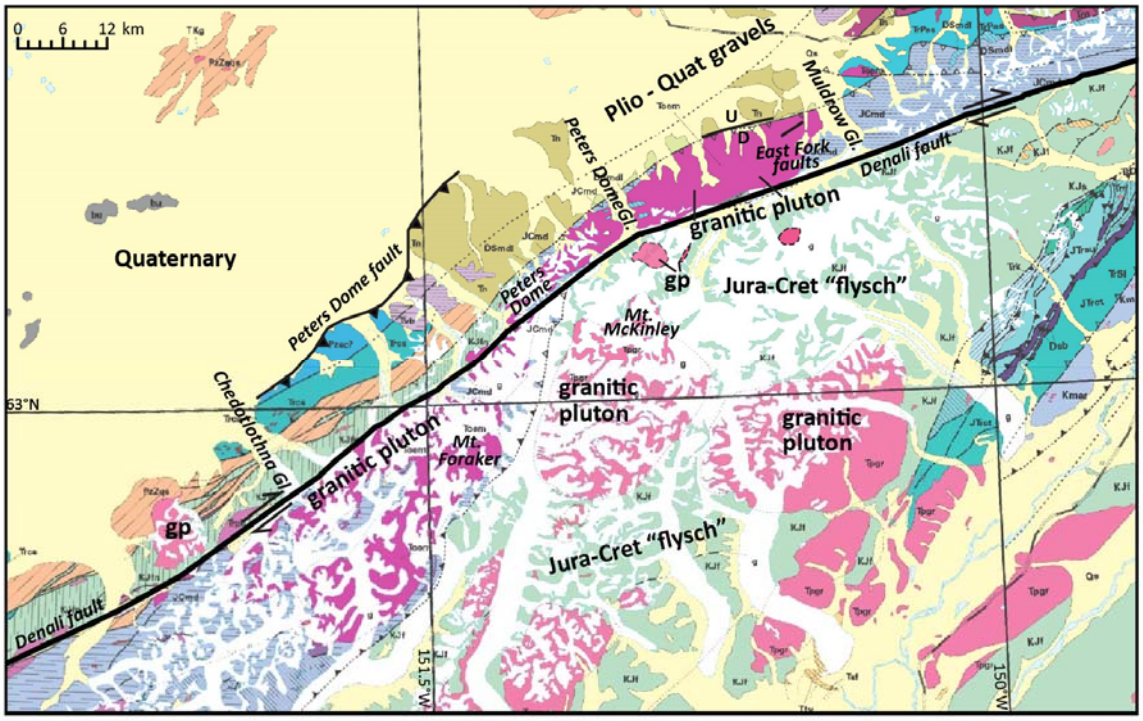

Figure 1.3: A simplified geologic map of the Mount McKinley restraining bend. Modified from Wilson et al. (1998). The late Quaternary faults are annotated and the Denali fault is bold. Also shown are generalized bedrock classifications, highlighting the occurrence of a variety of granitic plutons (also "gp") within the larger body of the Kahiltna Assemblage (the Jura-Cretaceous flysch). White map units are glaciers. The Denali fault has an overall westward decrease in slip rate (Matmon et al., 2006; Meriaux et al., 2009) and preliminary results from Haeussler et al. (2012), suggests that this slip rate decreases further across the MMRB.

1.2 Research Questions

The strongly asymmetric topography across the through-going strike-slip fault of the MMRB results in an abrupt contrast in the development and preservation of markers for the study of Quaternary tectonics, with the north side containing a Quaternary sequence of landforms and deposits and superimposed active structures and the south side dominated by glaciers and steep bedrock cliffs.

The geomorphic preservation of these structures north of the Denali fault presents an opportunity to address questions related to the active deformation and evolution of this restraining bend system. In this study, I attempt to address 4 primary questions: 1) Is there a change in faulting style across the apex of the restraining bend that corresponds with the increase obliquity of motion to the northwest (Figure 1.4)? 2) Does a spatial relationship exist between the distribution of earthquake events and the locations of faults across the apex (Figure 1.5)? 3) How much of the slip budget for the MMRB system is accommodated by faults north of the Denali fault (Figure 1.6)? 4) How is the Mount McKinley restraining bend evolving (Figure 1.6)? To address these questions I will need to document the distribution of Quaternary deposits and establish age control and correlations to provide a framework for characterizing active fault locations and geometries and determining deformation rates. From this I will establish a comprehensive understanding of the timing, distribution, and geometry of the faults in relation to location of the faults to the apex of the bend. Finally, I will shed light on the seismicity of the MMRB associated with the active faults and define the structure of the faults at depth to complete the first order understanding of how the MMRB is evolving.

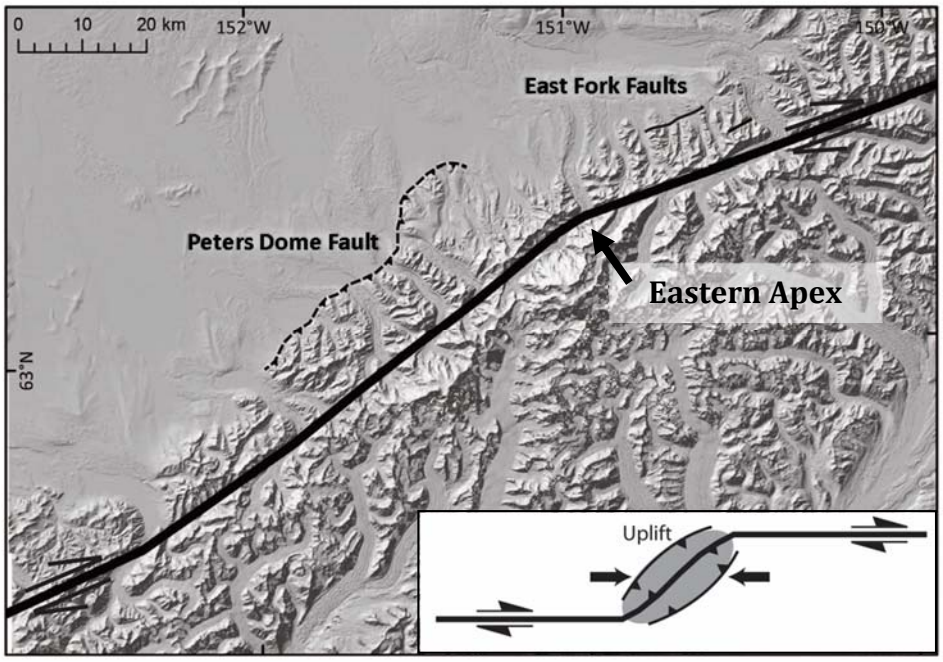

Figure 1.4: Research question 1. Is there a change in faulting style across the eastern apex of the restraining bend that corresponds with the increase obliquity of motion to the northwest? The inset figure shows the general structure and deformation of a restraining bend. This schematic structure is similar to what we see on the Denali fault above. The Denali fault near the East Fork fault is a straight segment like the right side of the inset figure. To the west, the Denali fault bends abruptly to the southwest; I will refer to this point along the Denali fault as the 'apex' of the restraining bend. The Mount McKinley restraining bend extends from the apex to another relatively discrete bend ~70 km to the southwest where then the Denali fault regains a WSW-ENE trace that is relatively parallel to the east of the apex. Deformation resulting in uplift, according to the inset figure, occurs mainly adjacent to the more SW-NE oriented portion between the fault bends. I want to determine if faulting style changes across the apex.

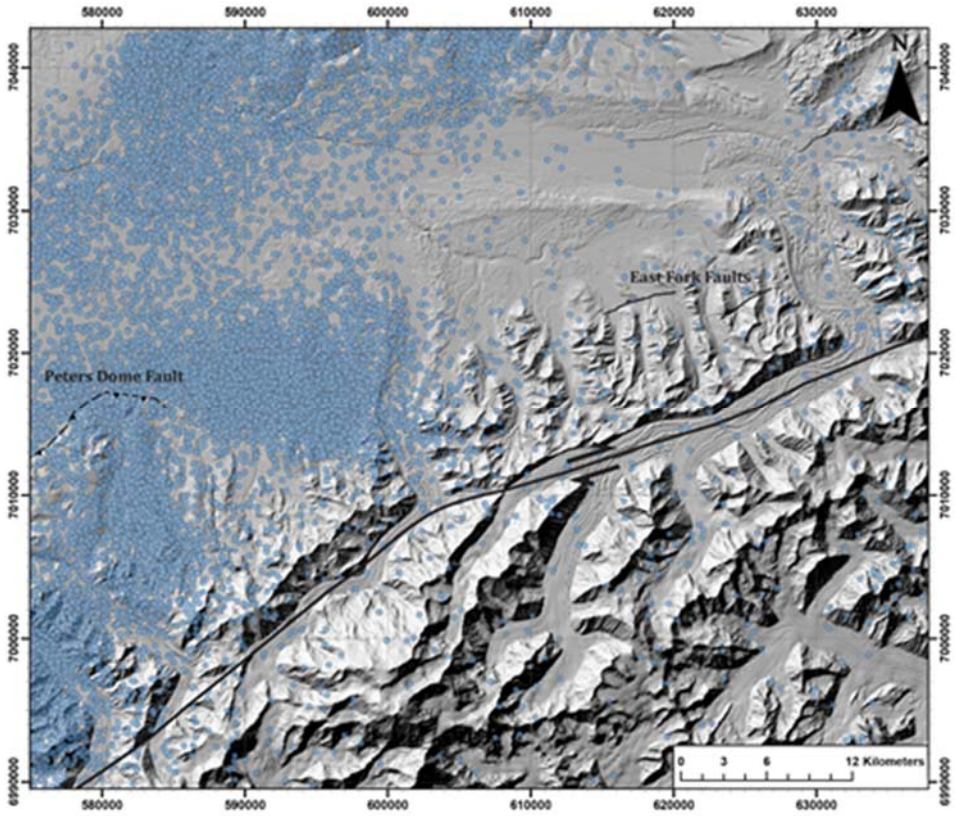

Figure 1.5: Research question 2. Does a spatial relationship exist between the distribution of earthquake events and the location of Quaternary faults across the apex? There is a distinct pattern in seismicity with the hypocenters being clustered north and to the west of the eastern apex of the Denali fault with a lack of seismicity occurring to the east of the eastern apex near the East Fork faults. Geology usually displays patterns and through this project, I want to know what these hypocenter patterns can say about the Mount McKinley restraining bend.

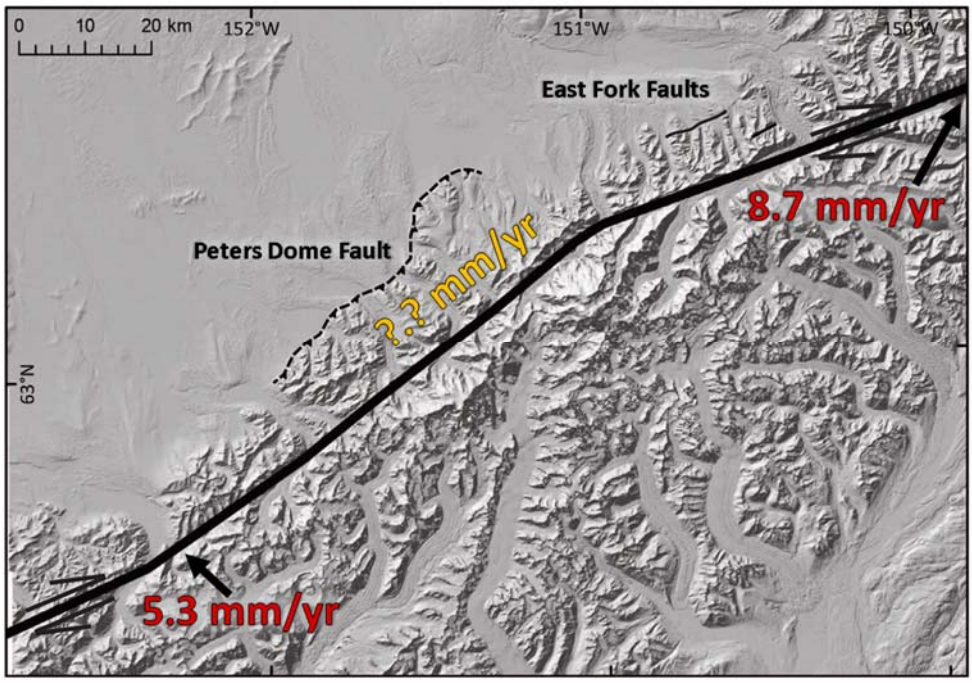

Figure 1.6: Research question 3 and 4. 3) How much of the slip budget for the MMRB system is accommodated by faults north of the Denali fault? The lateral slip rate on the Denali fault is decreasing to the west (Matmon et al, 2006). The formation of the foothills north of Denali is evidence of strain partitioning onto active structure from the Denali fault to accommodate the uplift of these foothills. This project hopes to define the amount of horizontal shortening occurring on the active faults north of the eastern apex of the MMRB to account for a portion of the lateral slip rate decrease on the Denali fault. 4) How is the Mount McKinley restraining bend evolving? The possible abrupt change in faulting correlating with patterns in seismicity along with decrease in lateral slip rates are all evidence of an evolving Mount McKinley restraining bend.

CHAPTER TWO: SETTING

2.1 Geologic Setting

Alaska has been built by terrane accretion associated with transported continental fragments and island arcs colliding with the southern Alaska plate margin. The boundaries between these accreted fragments are sewn together by intra-continental suture zones (Trop and Ridgway, 2007). As highly deformed and relatively weak crustal boundaries (e.g. Dewey, 1977), suture zones can focus long-term, high magnitude displacement on major intracontinental shear zones forming within the suture boundary. The Yakutat microplate is the most recent of these exotic terranes to collide with Alaska and is currently subducting as a thickened part of the Pacific plate beneath the North American Plate (Eberhart-Phillips, 2006). The plate collision, accretion, and flat-slab subduction along southern Alaska drives the transfer of stress >500 km inward to central Alaska. This transferred stress is manifest as widespread crustal seismicity in south-central Alaska and the formation of the Alaska Range. In particular, the Denali fault, which appears to have formed within the Alaska Range suture zone (Ridgway et al., 2002; Eberhart-Phillips, 2006), localizes much of this deformation along the fault trace and associated Alaska Range. (Jadamec et al., 2013; Bemis et al., in review).

The deformation along the Denali fault is accommodated by lateral slip and shortening, from partitioning of strain into the uplift of the central Alaska Range on numerous sub-parallel thrust faults of the northern Alaska Range thrust system. This thrust system is defined by Quaternary thrust faults and fault-related folds, forming a broadly arcuate basement-involved fold-thrust belt that parallels the trace of the

Denali fault (Figure 1.2; Bemis et al., in review). This understanding of active tectonics for the Alaska Range has recently evolved with the recent mapping of these faults from a variety of imagery including digital elevation models, aerial photography, and others (Bemis et al., 2012; Bemis and Wallace, 2007). Predominantly, the Alaska Range is strongly asymmetric in terms of topography with wide, broad swath of tall, rugged, glaciated peaks being north of the Denali fault with the superimposed thrust faults, while the south side of the Denali fault is dominated by narrow bands of foothills and local peaks. This trend changes going west along the Denali fault into the Kantishna Hills zone (Figure 2.1) where the topographic and deformational asymmetry reverses, forming a narrow band of foothills, the Peter Dome foothills, to the north of the Denali fault opposed to the broad, strongly deformed Mount McKinley region to the south.

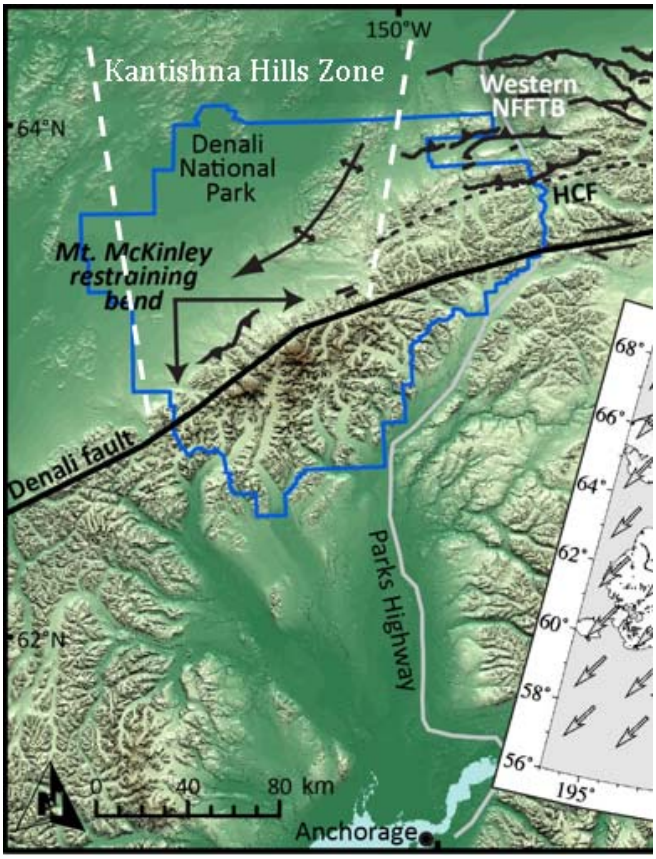

Figure 2.1: Kantishna Hills zone. A deformation zone that starts where the thrust faults of the Alaska Range to the east terminate at the Kantishna Hills anticline. The active deformation of the Kantishna Hills zone is currently characterized by three structures: the Kantishna Hills anticline, Peters Dome fault, and the East Fork faults.

The active deformation of the Kantishna Hills zone is currently characterized by three structures: the Kantishna Hills anticline, Peters Dome fault, and the East Fork faults (Figure 2.1). The Kantishna Hills anticline is an actively deforming structure oblique to the thrust faults of the northern Alaska Range thrust system that lies immediately to the east. The broad and gently asymmetry geometry of this anticlinal fold suggests that it is underlain by an active thrust fault, but evidence from previous research has not recognized a surface trace for such a fault (e.g., Bemis and Wallace,

2007). The Peters Dome fault is a recently recognized, south-dipping thrust fault which underlies an uplifted plateau-like landform and defines at least 15 km of the topographic range front through the Peter Dome foothills (Bemis et al., 2012). The other previously mapped Quaternary-active fault in this region, the East Fork faults (Plafker et al., 1994), offset the foothills to the west of Muldrow Glacier and are documented as two short fault traces with young geomorphic scarps (Figure 1.3). The geologic setting and regional bedrock mapping suggest that there should be additional active faults along the Peter Dome foothills. Reed (1961) describes parallel faults that control long topographic depressions and offsets between pre-Tertiary units along the foothills in the report that accompanies his regional map, but these active fault traces are not depicted. Also in the regional-scale mapping, Reed (1961) documents a continuous fault mapped in bedrock through the foothills along front of the foothills between the Muldrow Glacier and the Straightaway Glacier further supporting additional faults. These active faults would be necessary to accommodate the shortening that formed the Peters Dome foothills with the active deformation of the Denali fault.

The bedrock geology of the Peters Dome foothills consists of poly-metamorphosed Precambrian to Paleozoic rocks of the Yukon Tanana terrane, Cretaceous and Tertiary sedimentary rocks, and Paleocene to Eocene volcanics (Reed, 1961). These units are extensively deformed and intruded by dikes and granitic plutons (e.g., Reed, 1961; Ridgway et al., 2007) of Mesozoic age around 38 Ma (Reed and Lanphere, 1974). North of the Denali fault and within the Peters Dome foothills is the Hines Creek fault, which is a major crustal boundary that represents the

northern margin of the Alaska Range suture zone (e.g., Ridgway et al., 2007; Brennan et al., 2011) (Figure 2.2). As the margin of the suture zone, this fault separates the Precambrian/Paleozoic rocks of the former North American continental margin from Mesozoic accreted terranes and related deposits. Late Cretaceous sedimentary rocks of the Cantwell formation represent a basin formed across the Alaska Range suture zone during the waning phases of the associated terrane accretion episode. The Cantwell formation is unconformably overlain by the Paleogene Teklanika formation (also known as the Upper Cantwell formation) which is a sequence of volcanic rocks consisting of andesite and rhyolite with some basalt and pyroclastic rocks (e.g. Peterson 1961; Gilbert et al., 1976). Collectively, the Cantwell and Teklanika formations constitute the Cantwell basin which is primarily preserved between the Denali and Hines Creek faults (Reed, 1961; Csejtey et al., 1992). In the Peters Dome foothills, the only mapped geologic units younger than the Teklanika formation are the Plio-Pleistocene Nenana Gravel and the sequence of Quaternary glacial and surficial deposits.

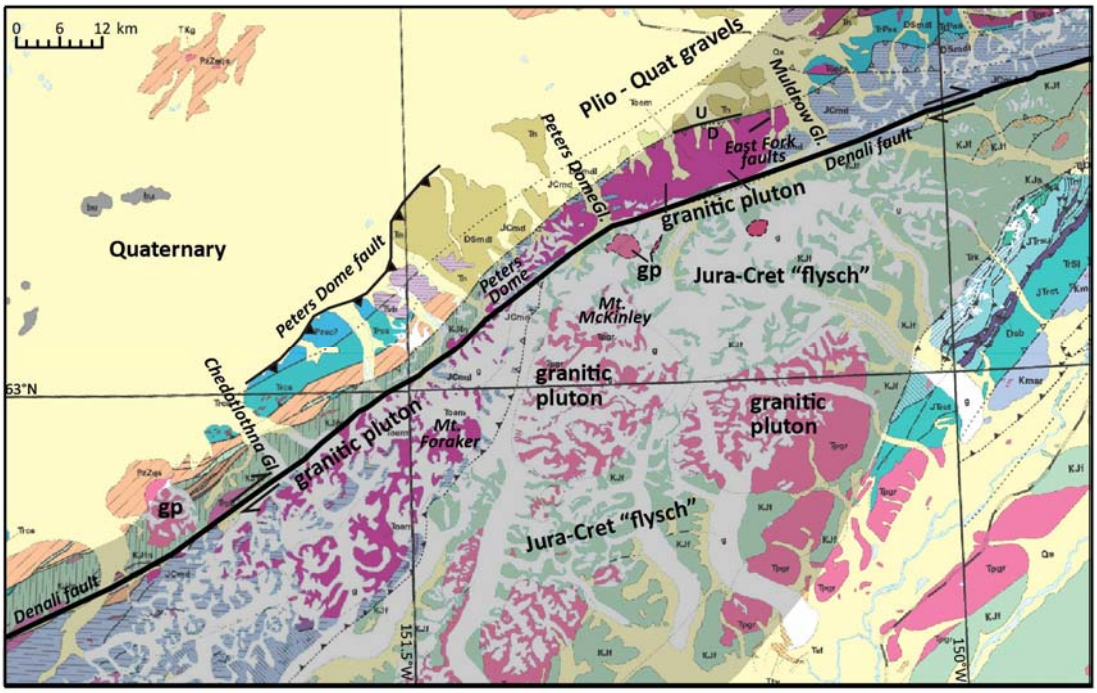

Figure 2.2: Alaska Range suture zone. The suture zone is defined by the black transparent overlay on the geologic map of the Mount McKinley restraining bend. The Denali fault formed in the highly deformed Alaska Range Suture Zone which is bounded to the north by the Hines Creek fault. This northern boundary is represented by the boundary between older Precambrian and Paleozoic metamorphic rocks from younger Mesozoic accretionary mélange labeled Jura-Cret "flysch" or KJf. The southern boundary is defined by a similar trend, but is more complex boundary.

The Kantishna Hills zone includes the area defined by the seismicity of the Kantishna Cluster, with the abundant earthquake hypocenters overlapping a significant portion of the study area. Particularly vexing for seismologists are that despite the abundant shallow crustal seismicity, there are no previously-mapped active faults that correspond with the style and trends of the Kantishna Cluster (Burris, 2007). To characterize the seismogenic character of the crust in this region, Ruppert et al. (2008) used relocated earthquake hypocenters, to conclude that

seismicity in the cluster rarely extends deeper than 12 km. This indicates that this depth is the seismic limit of the crust. Two clusters of earthquake hypocenters trending about SW-NE and WNW-ESE defined the Kantishna Cluster during the beginning analysis of the cluster in the early 2000s, with the northern section showing mainly reverse/thrust slip and strike-slip focal mechanisms while the southern section showed mainly right lateral strike-slip focal mechanisms (Ratchkovski and Hansen, 2002). Continued analysis of the Kantishna Cluster has led to the identification of 3 primary subzones of seismicity: the north, middle, and south zone, distinguished by defined sub-clusters of earthquake hypocenters inside the large Kantishna cluster and their specific orientation to the Denali fault (Figure 2.3; Ruppert et al., 2008; Burris, 2007). The north and south zones of cluster earthquake hypocenters are orientated parallel to the Denali fault along the restraining bend, while the middle zone is orientated oblique to the restraining bend. The majority of deformation is accommodated by strike-slip and reverse/thrust slip evident by the focal mechanisms in the zones. (Ratchkovski and Hansen, 2002; Burris, 2007; Ruppert et al., 2008). These zones of deformation highlight the complexity of the Kantishna Cluster that we hope to advance the understanding of by providing new constraints on the underlying faults.

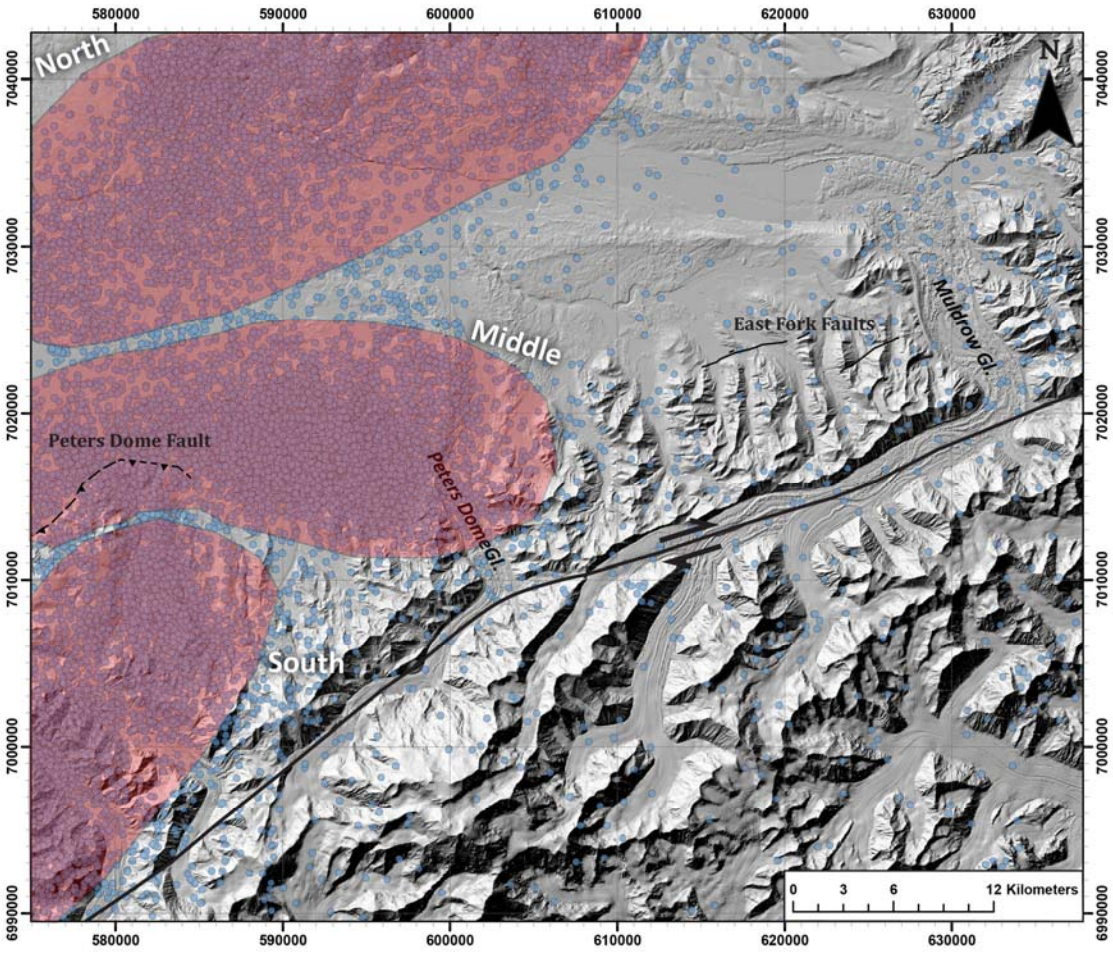

Figure 2.3: Seismicity near the Mount McKinley restraining bend. The seismic phenomena north of the Mount McKinley restraining bend is called the Kantishna Cluster. There are 3 recognized zones of seismicity (Burris, 2007; Ruppert et al., 2008) of the cluster, and they are called the north, middle, and south zones. Seismicity is minimal east of Peters Dome Glacier to the Muldrow Glacier despite the occurrence of mapped Holocene-active faults. The highest magnitude earthquake for the cluster (M5.2) occurred in 2011 at the northern tip of the north zone.

CHAPTER THREE: METHODOLOGY

3.1 Research Methods

I conducted surficial and neotectonic geology mapping of the Peter Dome foothills at 1:24,000 scale targeting the late Cenozoic geologic record associated with restraining bend deformation. The existing mapping was conducted at 1:250,000 scale and largely prior to the publication of the systematic topographic map coverage for the region (Reed, 1961), and provides a general framework for the regional geology, but there is significant room for improvement. My mapping efforts consisted of initial reconnaissance-level mapping on satellite imagery and moderately high-resolution topography in ArcGIS, 1 week of fieldwork in summer 2013 (this was shorter than planned due to sickness of a colleague), detailed mapping and integration of field observations in ArcGIS, and the compilation of a final map. Imagery used for mapping included aerial photography, satellite images, moderately high resolution digital elevation models, and pre-existing geologic maps. Despite the limited duration and coverage of the fieldwork, it provided a key opportunity to check preliminarily mapped contacts and units and to characterize the types of deposits associated with different vegetative patterns, landforms, and surface textures observable on the remotely-sensed data to facilitate accurate unit identification across the regions I could not access directly to include the undifferentiated bedrock, Pliocene Nenana gravel, Quaternary deposits, and faults.

For age control on the surficial deposits, I used mapped relationships of Reed (1961), Wahrhaftig (1958), and Dortch et al., (2009; 2010) to make regional correlations of the glacial moraines of the Alaska Range to the moraines present along

the Peter Dome foothills to establish preliminary constraints on the mapped landform and deposit ages. For these deposits I mainly focused on the landforms that were offset by the faults to establish constraints on the timing and rate of slip on the faults. The new surficial geologic mapping highlighted these offsets in the mapped units and other fault-related geomorphic signatures.

The geomorphic signatures were then used to precisely map new faults of the foothills. The faults were mainly mapped by fault scarps that offset the surficial deposits. I selected well-preserved fault scarps with clear hanging wall and footwall surfaces along McLeod Creek and Slippery Creek to characterize the strain north of the eastern apex. I surveyed perpendicular topographic profiles (Figure 3.1) across these scarps to define their scarp structure and to calculate a slip rate for the fault associated with the scarps. The surveys were performed with a hand-held Trimble 6000 series GPS unit having an optimal precision of 10 centimeters. A point spacing of 5-10 m was used along the hanging wall and footwall with closer spacing when crossing the scarp face. For a more accurate constraint on the age of the surface offset by the Slippery Creek scarp, I collected radiocarbon samples below the Slippery Creek 2 fault scarp. The surveys gave me a topographic profile and from that I derived the slip offset along the fault plane separating the hanging wall and footwall. Once the slip vector was calculated I divided it by the estimate surface age from the glacial correlations to obtain a slip rate. Finally, I visualized the active faults and their relationship to the focal mechanism and earthquake data for all record events from 1968 to 2013 by overlaying the faults on the seismicity. The overlay of faults and seismicity was displayed in ArcScene with USGS's 3-D visualization of earthquake

focal mechanism program created by Labay and Haeussler (2007) and used to highlight focal mechanisms trends, distribution of seismicity, and link the seismicity with the known faults. Also cross sections of the earthquake hypocenters were made through the Kantishna Cluster to image the subsurface structure related to the seismicity.

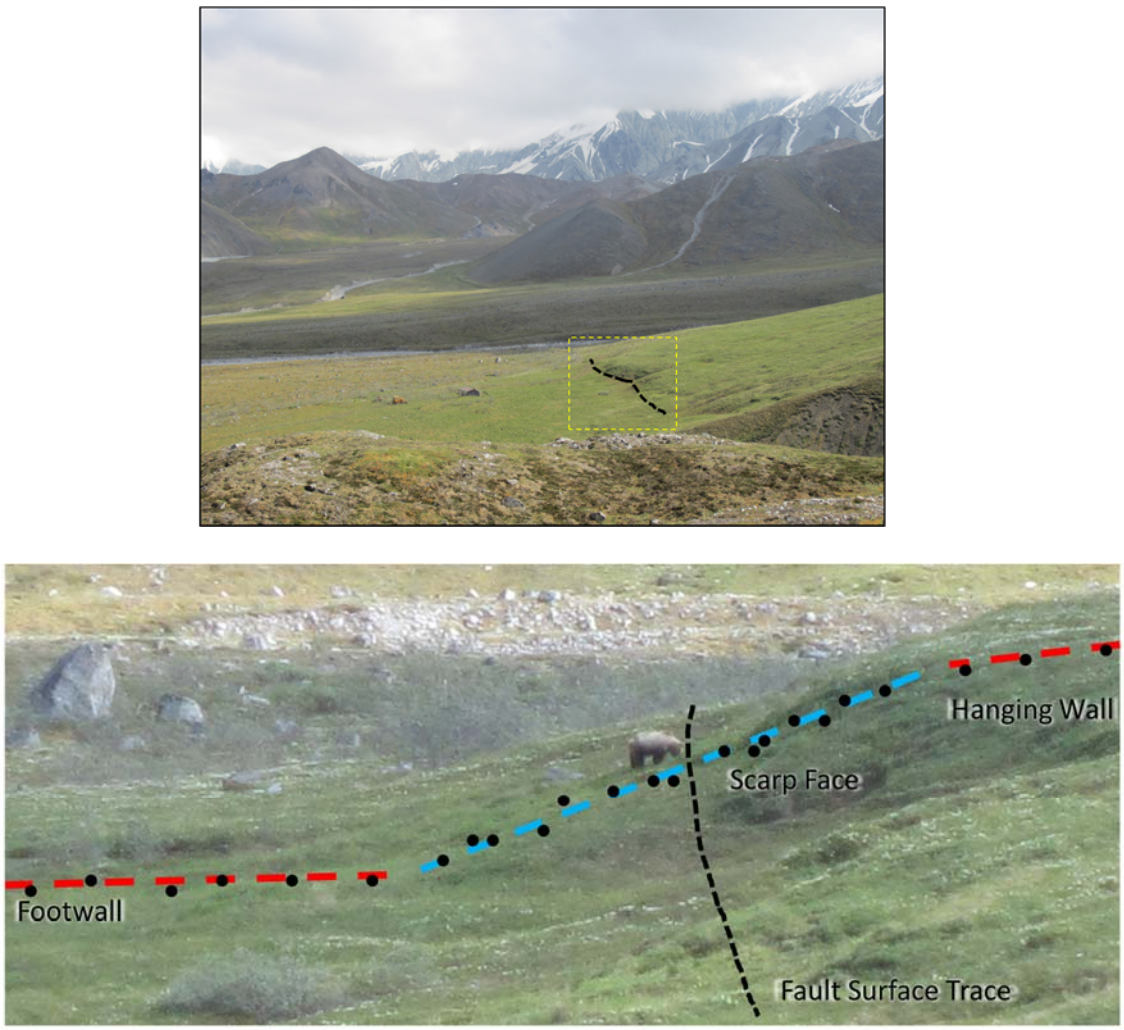

Figure 3.1: Topographic profile example. A) Is an aerial photo of a fault scarp offsetting alluvial deposits on the west fork of Slippery Creek. The yellow dashed box defines the area of the bottom photo. B) This is a zoomed in photo of the previous fault scarp. There is a bear here for scale. The red dash lines represent the hanging wall and footwall surfaces. While the blue dashed line shows the scarp face. These lines were defined by the gps points (black dots) that correspond to each surface. All the gps points make up a topographic profile.

CHAPTER FOUR: RESULTS

4.1 Quaternary Geology

The stratigraphy of the MMRB region can be subdivided into 3 primary components, 1) undifferentiated bedrock composed of metamorphic, igneous and sedimentary rocks. 2) Pliocene Nenana Gravel, 3) Quaternary glacial, alluvial, and colluvial deposits and landforms that are broadly correlative with major climatic events. I separated the Quaternary deposits based on Reger et al. (2012), nomenclature and descriptions. Even though Reger et al. (2012), maps are not near my study area, they depict a similar geologic and geomorphic setting with active and recent glacial geomorphology superimposed upon Quaternary deformation. I mapped all unit contacts as approximate since they were mapped using high resolution imagery and limited field mapping (Figure 4.1). General descriptions of the units are provided below, with more detailed descriptions provided in Table 4.1.

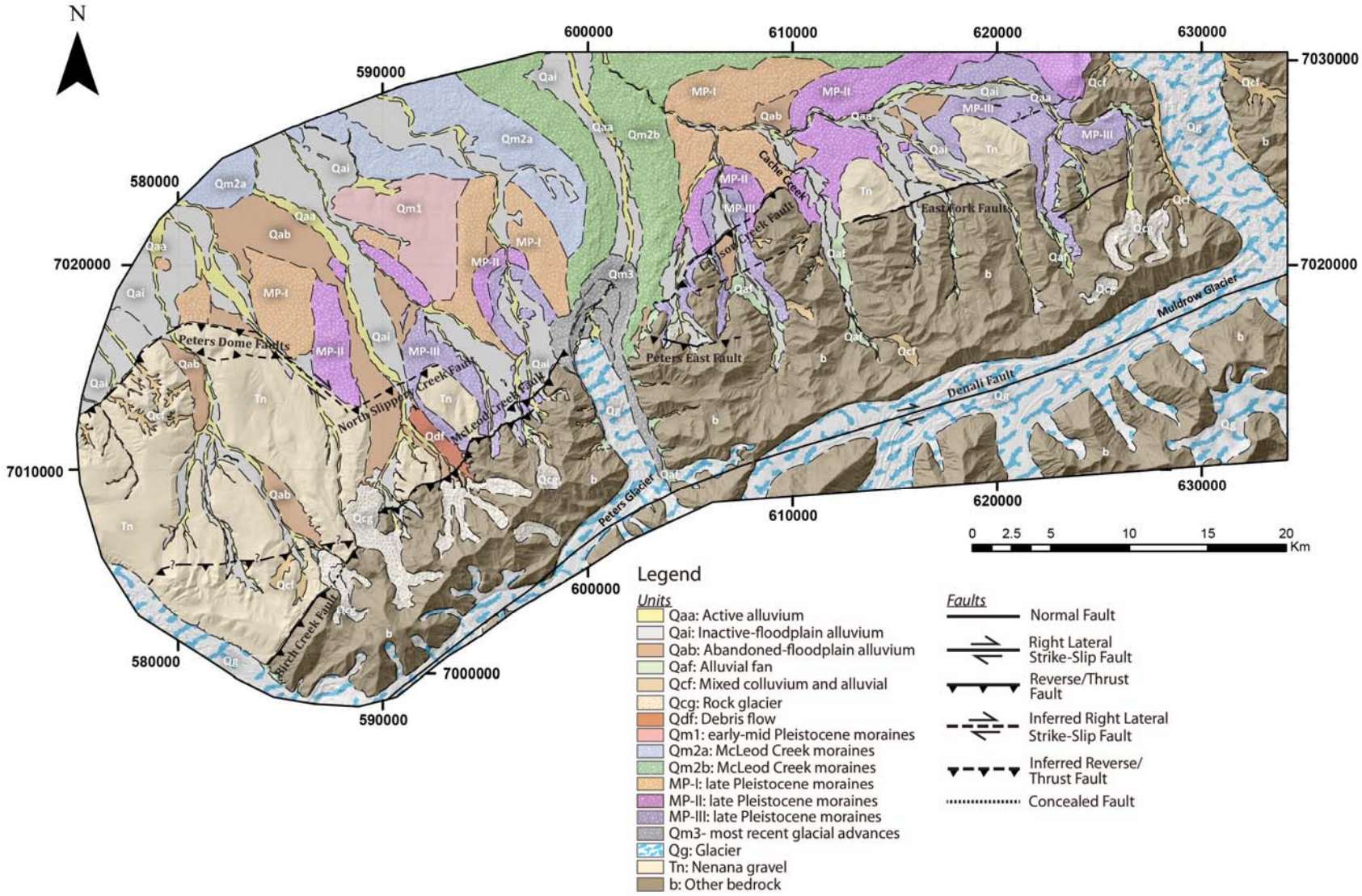
N
600000
610000
620000
630000
590000
7030000
580000
7020000
7010000
7000000
Peters Dome Faults
North Slippery Creek Fault
McLeod Creek Fault
Peters East Fault
Cache Creek
Carlson Creek Fault
East Fork Faults
Muldrow Glacier
Denali Fault
Peters Glacier
Birch Creek Fault
0 2.5 5 10 15 20
Km
Legend
Units
Qaa: Active alluvium
Qai: Inactive-floodplain alluvium
Qab: Abandoned-floodplain alluvium
Qaf: Alluvial fan
Qcf: Mixed colluvium and alluvial
Qcg: Rock glacier
Qdf: Debris flow
Qm1: early-mid Pleistocene moraines
Qm2a: McLeod Creek moraines
Qm2b: McLeod Creek moraines
MP-I: late Pleistocene moraines
MP-II: late Pleistocene moraines
MP-III: late Pleistocene moraines
Qm3- most recent glacial advances
Qg: Glacier
Tn: Nenana gravel
b: Other bedrock
Faults
Normal Fault
Right Lateral Strike-Slip Fault
Reverse/Thrust Fault
Inferred Right Lateral Strike-Slip Fault
Inferred Reverse/ Thrust Fault
Concealed Fault

Figure 4.1: Surficial geology and Quaternary fault map. Map of the surficial geology and Quaternary faults of the Peter Dome foothills. The faults are mainly range flanking faults found at the farthest extend of the active foothills of the range. The thrust faults transition in nearly vertical dip slip faults after Cache Creek to the Muldrow Glacier except for the range flanking thrust faults. The solid black line right-lateral fault at bottom of figure is the Denali Fault.

Undifferentiated Bedrock- b

Reed (1961) mapped the Peter Dome foothills of the Alaska Range, as stated in the geologic setting, as poly-metamorphosed Precambrian to Paleozoic rocks of the Yukon Tanana terrane, Cretaceous and Tertiary sedimentary rocks, and Paleocene to Eocene volcanics, that were deformed and intruded by dikes and granitic plutons (Reed, 1961). New data is not presented in this study on undifferentiated bedrock due to my focus was on the Quaternary stratigraphy and deformation.

Pliocene Nenana Gravel- Tn

The Nenana Gravel is a widespread Neogene sedimentary formation in the northern foothills of the Alaska Range. As a coarse-grained sequence of alluvial fan and braidplain deposits, this unit contains the foreland basin record of the early growth of the modern Alaska Range (e.g., Ridgway et al., 2007). The unit was uplifted and exposed by the northward propagation of the northern Alaska Range thrust system (Bemis and Wallace, 2007). In several regions across the Alaska Range, local conditions have preserved the upper surface of the Nenana Gravel where the former basin surface has passively uplifted on the hanging wall of a thrust fault and local exhumation has been minimal. In the Peters Dome foothills, the deposits correlated with the Nenana Gravel are characterized by plateau-like surfaces and smooth ridges (Figure 4.2). These characteristics permit the uplifted surface of Nenana Gravel to be used as an important marker for fault displacement and geometry. So when there is a bedrock contact between Nenana gravel and another bedrock unit in the foothills, then that contact has been a fault trace. The

unit tends to define the hanging wall surface of these faults and these faults are commonly not the main range bounding faults along the foothills.

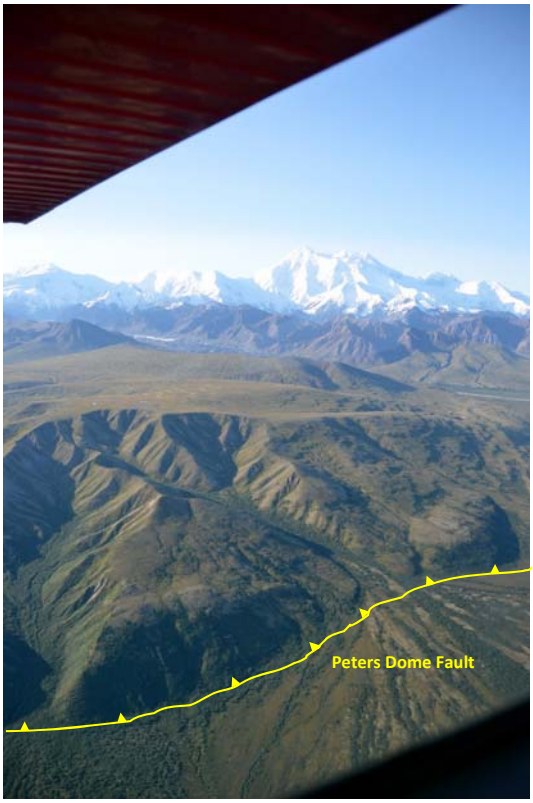

Figure 4.2: Nenana gravel plateau surface. View to the southwest across the Peters Dome fault. The Peters Dome fault flanks the front of this plateau.

Quaternary deposits

Most of the Quaternary deposits mapped in the Peters Dome foothills are associated with major glacier fluctuations of the mid to late Pleistocene and appear to reflect a similar glacial sequence as has been documented elsewhere in the Alaska Range (e.g. Wahrhaftig, 1958; Reger et al., 2008). The Peter Dome foothills are transected by several large modern glaciers that are sourced in the high peaks south of the Denali fault whereas the numerous cirque and small valley glaciers have smaller accumulation areas and are limited to the north side of the Denali fault. Glacier deposits are widespread throughout the foothill valleys and on the lowlands to the north. The extent of glaciers during the Last Glacial Maximum (LGM) is evident by the glacial moraine deposits that line the valley walls (MP-III), while other moraine deposits (MP-I, MP-II, Qm1, Qm2a, Qm2b) cover the lowlands and plains to the north. The McKinley Park glacial episodes (e.g. MP-I) were mapped from Dortch et al., 2009 and extend to the foothills west of the apex by mapping similar morphology of the moraine deposits. The other glacial episodes (Qm1, Qm2a, Qm2b) were all mapped by Reed (1961) and by differences in morphology and superposition. The differences in morphology are not characteristics that can be described as it was just the matching of deposits with similar textures while most deposits had similar characteristics of hummocky terrain and kettle lakes.

With moraine deposits derived from the regional glaciations blanketing the foreland to the north, the majority of the alluvial deposits are preserved near the foothills (Figure 4.3; 4.4). Almost all moraine deposits have been cut by actively eroding streams depositing active alluvium (Qaa). Along these active streams, non-active floodplains are defined from the active floodplain by cross cutting and

elevation relationships to the adjacent surfaces (Qai, Qab). Lining the bedrock streams of the foothills are a mixture of colluvium and alluvium deposits (Qcf). These stream cause a large sediment flux to form large single and coalescing alluvial fans (Qaf) along the flanks of main drainage valleys, commonly dissecting and covering glacial deposits. Rock glacier deposits (Qcg) are restricted to the peak areas of the foothills, where there are some that are waning remnants of former real glaciers and others that formed from empty spaces of colluvium being filled with ice allowing for the mixture to move down slope.

Table 4.1 – Surficial unit descriptions

	Unit	Description
Alluvial	Active Alluvium (Qaa)	Qaa are active channel deposits, that were mapped based on base level of the river and represents the transition from active channel to floodplain or next elevated surface. Braided streams bars and directly adjacent floodplains were consider active alluvium.
	Inactive-floodplain alluvium (Qai)	Qai are the previous floodplain that is commonly the next elevated surface up from the active alluvium and had very little vegetation. This is a late Holocene floodplain.
	Abandoned-floodplain alluvium (Qab)	Qab are the highest surfaces along the inside of a drainage that are smooth on lidar, but have more substantial vegetation than Qai. These are older, abandoned floodplains compare to the Holocene floodplains of Qai.
	Alluvial fan deposit (Qaf)	Qaf are fan-shaped deposits that line the edges of the ridges and are commonly coalescing.
Colluvial	Mixed colluvium and alluvium deposit (Qcf)	Qcf are a deposit lining the bedrock stream drainages of the foothills. The slopes of the drainage are commonly talus slopes so the contact between the alluvial and colluvial deposits is gradational forming a deposit that includes a mixture of colluvium and alluvium.
	Debris flow deposit (Qdf)	Qdf is a debris flow deposit distinguished by its abundant boulder cover on the ground surface.
	Rock-glacier deposit (Qcg)	Qcg are glacier like deposits restricted to the peak areas of the foothills, where there are some that are waning remnants of former real glaciers and others that formed from empty spaces of colluvium being filled with ice allowing for the mixture to move down slope.
Glacial	Glacial deposit (Qg)	Qg are the active glaciers where the majority of the deposit is ice.
	Qm1	Qm1 is a smooth moraine deposit located north of the McLeod Creek scarp between McLeod creek and Slippery Creek. It has a hummocky terrain with no kettle lakes. This is an early-mid Pleistocene age moraines.

Table 4.1 – Surficial Unit Descriptions (Continued)

Glacial	Qm 2a	Qm 2a are McLeod Creek moraines previously mapped by Reed (1961).
	Qm 2b	Qm 2a are McLeod Creek moraines previously mapped by Reed (1961).
	MP-I	MP-I are late Pleistocene moraines previously mapped by Ten Brink and Waythomas (1985) and newly mapped moraines interpreted from the texture and superposition of the moraines mapped by Ten Brink and Waythomas (1985).
	MP-II	MP-II are late Pleistocene moraines previously mapped by Ten Brink and Waythomas (1985) and newly mapped moraines interpreted from the texture and superposition of the moraines mapped by Ten Brink and Waythomas (1985).
	MP - III	MP-III are late Pleistocene moraines previously mapped by Ten Brink and Waythomas (1985) and newly mapped moraines interpreted from the texture and superposition of the moraines mapped by Ten Brink and Waythomas (1985).
	Qm3	Qm3 are the most recent glacial advances during the Quaternary for Peters Glacier.
Bedrock	Nenana Gravel (Tn)	Tn is a coarse-grained alluvial sequence that filled the former Alaska Range foreland basin and in imagery the surface appears to be a smooth plateau surface.
	Other Bedrock (b)	Other Bedrock are poly-metamorphosed Precambrian to Paleozoic rocks, Cretaceous sedimentary rocks, and Paleocene to Eocene volcanics, felsic dikes and granitic plutons that have a rock like appearance in imagery.

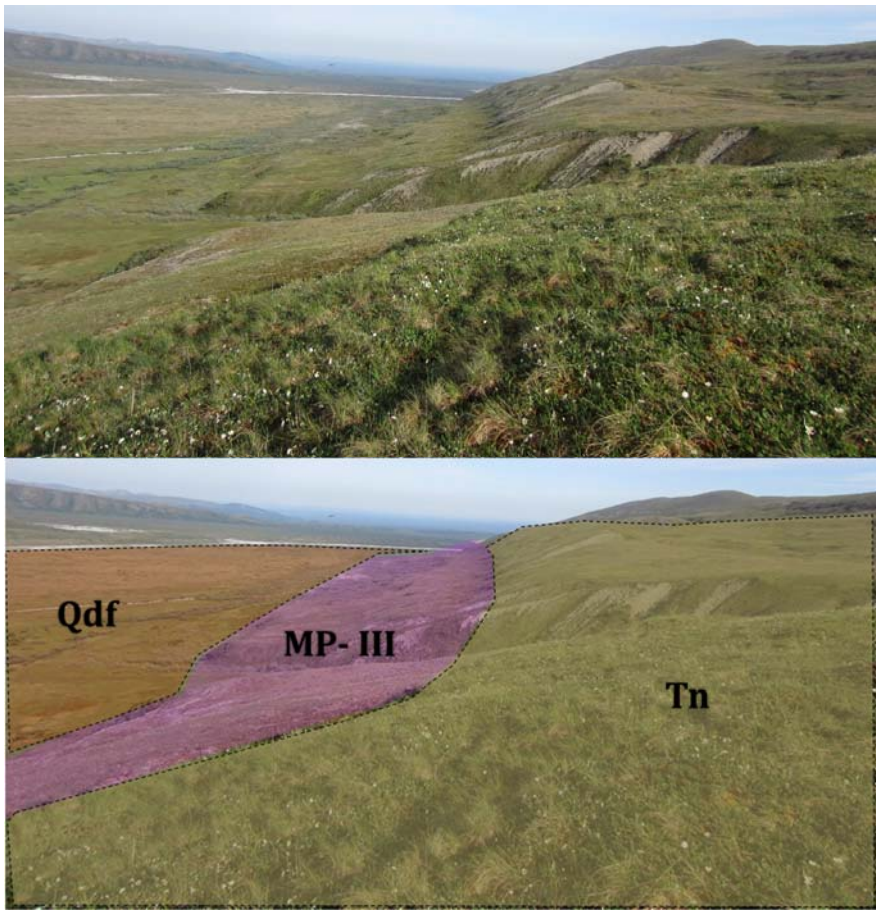

Figure 4.3: Field photo one of surficial deposits. View to the north on the edge of the east fork of the Slippery Creek drainage and shows how the moraine deposits flank the valleys and appear as steps into the valley.

Figure 4.4: Field photo two of surficial deposits. View to the east across the west fork of the Slippery Creek drainage and shows one of the prominent debris flows deposits distinguished by its abundant boulder cover. The figure also illustrates what some of the surficial deposits look like in the field area and how these deposits characterize the topography.

4.1.1 Age Control

The Alaska Range was not covered by a continental ice sheet during the Pleistocene glaciations allowing for a complex moraine sequence to dominant landforms of the Peter Dome foothills (e.g. Wahrhaftig, 1958; Ten Brink and Waythomas, 1985). Quaternary climatic variations in the late Pleistocene led to the valleys across the northern Alaska Range to have a long history of glaciations, with the most recent and best preserved of these being the early and late Wisconsin advances (Briner and Kaufman, 2008). The late Wisconsin pulse left behind the moraines inside Denali National Park (e.g., Dortch et al., 2009). Glacier retreat associated with this glacial advance occurred between 22 to 19 ka based on Ten Brink and Waythomas (1985) analysis correlating the glacial moraines with the Last Glacial Maximum (LGM) (28 to 19 ka). Reed (1961) extensively mapped the late Pleistocene glacier episodes along the McKinley River and the valleys of the Peters Dome foothills based on geomorphic characteristics. He called these moraines, the McKinley Park moraines (Dortch et al., 2009) and distinguished two separate advances. Later the moraines were divided into four advances: MP-I (~21.4-20.6 ka), MP-II (~20.6-19.9 ka), MP-III (~15.1-12.3 ka), and MP-IV (~12.3-11 ka) (Ten Brink and Waythomas, 1985).

I have assumed that the moraine surfaces of the Peter Dome foothills formed after the last glacial maximum since the oldest moraine occurring in this field area is MP-I at 21.4 to 20.6 ka. The active alluvium and floodplains of the foothills cut MP-II and MP-III moraines making the non-moraine surface ages closer to the Holocene age boundary (~12 ka). The younger MP-IV (~12.3-11 ka) is only present along the

McKinley River and north of the field area, so the age cannot be accurately bought closer to the present. Based upon previous statement parameters, I propose the maximum surface age of the non-glacial surficial surfaces to be Holocene to late Pleistocene in age (~12 ka). The maximum age will be used to calculate the absolute minimum slip rate possible for the mapped faults that offset these surficial surfaces or moraine surfaces. The relative ages of the glacial surficial surfaces (i.e. moraines) along the foothills are shown in Table 4.2.

Regional correlations were made with the McKinley Park moraines to frame the glacier episodes of the Peter Dome foothills in relation to other well defined glacial events of the Alaska Range. Briner and Kaufman (2008) correlates moraines of the Riley Creek 1 glacial advance with MP-I and the Riley Creek 2 advance between MP-I and MP-II. Riley Creek 1 occurred around 22-30 ka (Dortch, 2006) while Riley Creek 2 occur around 17-24 ka (Dortch et al, 2010). Riley Creek 1 and 2 occurred before the Carlo Creek moraines (e.g. Dortch, 2006) and in the late Wisconsin (e.g., Wahrhaftig, 1958). Carlo Creek glaciation is dated at 16.0 +/-1.8 ka (Dortch et al., 2010) and correlates with the Donnelly glaciation (~ 17-18 ka; Matmon et al., 2010) of the Delta River sequence. To put the glaciations of the foothills in context of global Quaternary climate fluctuations, the advance of mountain glaciers of the late Pleistocene in central and southern Alaska occurred during marine isotope stage 2 (Briner and Kaufman, 2008). These regional correlations add another constraint to the age control of the surfaces along the Peter Dome foothills already established by the previous mapped McKinley Park moraines.

Table 4.2: Glacial correlations

Mapped glacial deposit	Muldrow McKinley Park correlation #	Nenana River valley correlation ^	Delta River correlation <	Marine Isotope Stage correlation	Age range (ka) +	Alternative age correlation (ka)
Qm3	"X"/"Y" drift			MIS 1	<2	<2
MP-III	MP-III	Carlo Creek (16 ± 1.8 ka)	Donnelly (15-19 ka)	MIS 2	15.1 - 12.3	15.1 - 12.3
MP-II	MP-II	Riley Creek 2/ Carlo Creek	Donnelly (15-19 ka)	MIS 2	20.6 - 19.9	20.6 - 19.9
MP-I	MP-I	Riley Creek 1		MIS 2	21.4 - 20.6	21.4 - 20.6
Qm2a	McLeod Creek	Healy		MIS 4	57-71	57-64
Qm2b	McLeod Creek	Healy		MIS 4	57-71	64-71
Qm1*		Browne?		>MIS 6	>191	>191

* My Qm1 corresponds with the Qm1 mapped by Reed (1961), although he tentatively correlates Qm1 with the Healy advance of the Nenana River valley sequence. It appears that what Reed (1961) maps as Qm1 encompasses multiple older glacial advances based upon superposition of landforms and wide variation in moraine morphology (roughness, presence of kettles) between different moraines.

Correlations made based upon the summary by Dortch et al. (2009).

^ Correlations based upon Wahrhaftig (1958) and Dortch et al. (2010).

< Correlations based upon Matmon et al. (2010).

+ Ages derived from Dortch et al. (2009 ; 2010); Briner and Kaufman (2008); and correlations with the global marineisotope stages.

4.1.1.1 Carbon-14

I collected three block samples with disseminated stringers of black organic material from a natural exposure of the deformed stratigraphy associated with the McLeod Creek fault scarp at Slippery Creek (Figure 4.5; Figure 4.6). These stringers are part of the preserved ground surface below a major prehistoric debris flow that appears to have covered the valley floor and extended more than 3.5 km downstream. This rapid burial preserved a thin fine-grained horizon with organic material representing the pre-debris flow tundra and consisting of roots, wood, charcoal, and possibly seeds (small black spheres with a charcoal-like texture). A summary of the data from this buried soil, including radiocarbon ages, calibrated ages, scarp location, and significance of each sample is provided in Table 4.3. The samples were pretreated and measured at the Center for Accelerator Mass Spectrometry at Lawrence Livermore National Laboratory and the resulting radiocarbon ages were calibrated using OxCal v4.2 (Bronk Ramsey, 2009a) using the IntCal13 calibration curve (Reimer, 2013).

Due to a lack of individual macrofossils or charcoal fragments of sufficient size to date individually, I submitted five samples of different constituent components of the organic material from the buried soil. Each submitted sample was a collection of small fragments of similar types of material, either charcoal fragments, fine roots, woody fragments, or seeds(?). The sample of very fine roots provided an age indistinguishable from modern and is considered to be the result of roots from the modern tundra penetrating to ~1 m depth to the buried soil horizon. Three samples charcoal/charcoal-like material provided overlapping age ranges

that cluster around 3300 cal BP. These samples were the seeds(?) and the two separate samples of charcoal fragments. The sample consisting of small fragments of wood, twigs, and large roots provided an age around 630 cal BP. Stratigraphic and internal consistency of dated sample suggests that, despite each sample consisting of multiple individual fragments, each organic fraction within the buried soil horizon represents a relatively discrete period of time. With woody material being less stable in soils than charcoal, the radiocarbon ages appear to represent, 1) a tundra burning event at ~3300 cal BP; 2) continued soil development until the site is overridden by a debris flow shortly after ~630 cal BP; and 3) reestablishment of the tundra vegetation across the debris flow deposits.

Table 4.3: Radiocarbon age control on the Slippery Creek scarp

Sample Name*	CAMS Lab Number†	14C Age (BP)§	Calibrated age interval (cal BP)#	Sample material**	Sampled Unit	Significance
MMRB01-A	166184	3130 ± 140	3685 - 2960	Seeds? (a)	Organic Horizon	Max. limiting age
MMRB01-B	166185	>Modern	NA	Very Fine Roots (b)	Buried Soil	Disregard – unclear what was dated
MMRB01-C	166186	630 ± 70	684 – 525	Wood/Twigs/ Roots	Buried Soil	Min. limiting age
MMRB01-D ¥	166187	3065 ± 25	3359 – 3210	Charcoal (c)	Buried Soil	Max. limiting age
MMRB01-F	166188	3140 ± 60	3480 – 3182	Charcoal (c)	Buried Soil	Max. limiting age

Note: All analysis was done at LLNL CAMS.

* Site name codes: MMRB = Mt. McKinley Restraining Bend (01 = Slippery Creek topographic scarp profile 2)

† AMS analysis at the Center for Accelerator Mass Spectrometry (CAMS) at Lawrence Livermore National Laboratories.

§ The quoted age is in radiocarbon years using the Libby half-life of 5568 years and following the conventions of Stuiver and Polach (1977). Sample preparation backgrounds have been subtracted, based on measurements of radiocarbon-dead standards pretreated in parallel with samples.

Ages calibrated with Oxcal v4.2 (Bronk Ramsey, 2009a) using the IntCal 13 calibration curve (Reimer et al., 2013), with ages quoted at 2σ errors.

¥ Sample was large enough to take a sample specific aliquot for 13C analysis

** (a) black, charcoal-like spheres – origin unknown. (b) contaminated sample from modern roots penetrating buried soil horizon. (c) weathered charcoal of a previous surface that was likely transported, reworked, and rapidly buried during debris flow

588838
593838
7012566
7007566
N
North Slippery Creek fault
McLeod Creek fault
Slippery Creek
McLeod Creek
Qai
Qaa
MP-III
Tn
Qab
Qdf
Qcf
Qcg
b
1
2
3
Legend
Units
Qaa: Active alluvium
Qai: Inactive-floodplain alluvium
Qab: Abandoned-floodplain alluvium
Qaf: Alluvial fan
Qcf: Mixed colluvium and alluvial
Qcg: Rock glacier
Qdf: Debris flow
MP-III: late Pleistocene moraines
Tn: Nenana gravel
b: Other bedrock
Faults
Reverse/Thrust Fault
Inferred Reverse/ Thrust Fault
Concealed Fault
0 0.35 0.7 1.4 2.1 2.8
Km

Figure 4.5: Map of the field area. Field area with the Northern Slippery Creek and McLeod Creek thrust faults. The linear orange dots are the topographic profiles taken perpendicular to the different scarp segments of the thrust faults along McLeod Creek and Slippery Creek. These profiles were used to measure the vertical offset of the fault to calculate the slip rate along each scarp's fault plane. The yellow star was base camp during fieldwork in the area. The background map is a hillshade of a digital elevation model. The units are explained in the legend.

Figure 4.6:Cross-section of the Slippery Creek scarp. A continuous layers of organics and clays are bulldozed in a common blind thrust style with an offset of the continuous layers occurring in line with the base of the scarp. A blowup of the offset is shown to the right. The orange lines follow the bottom of the organic and clay layers.

4.2 Structural Geology

Active faults have been successfully mapped by the recognition of visible fault scarps and offsets in geomorphic features that are visible on a variety of imagery along the Alaska Range (Bemis et al., 2012; Bemis and Wallace, 2007).The fault-related geomorphic signatures seen in the imagery and seismicity were the first-order clues of the widespread abundance of active faults along the Peters Dome foothills. The geomorphic signatures used to identify new faults, in this study, are fault scarps, trends in topographic highs, contacts between bedrock of different orientation, the abrupt range front of the foothills, different erosional patterns of adjacent bedrock, lineaments in satellite imagery, the uplift of Quaternary deposits, and plateau-like surface. I found that a majority of the new faults recognized during this mapping parallel the Denali fault, forming large fault segments. These segments are predominantly thrust faults, although a few normal faults and right-lateral strike-slip faults appear to define changes in fault geometry and strain accommodation patterns seen along the Peter Dome foothills (Table 4.4). In particular, my mapping illustrates a significant east-west change in active faulting style corresponding with the abrupt angular bend in the Denali fault (the 'east apex' of the restraining bend) (Figure 4.1).

Table 4.4: Summary of Quaternary faults of the Mt. McKinley restraining bend

Fault name	Activity*	Offset units	Geomorphic expression	Dip Direction	Dip (°)#	Relative motion	Source+
Birch Creek	Holocene	Qaa,Tn, b	Different Striking Bedrock, faint scarp	SE	15-45	SE-up	
Carlson Creek fault	Holocene	Qaa, Qai, Qgm, Qab, b	Fresh scarp	SE	15-45	SE-up	
East Fork fault (Northern)	Holocene	Qaa, Qaf, Qgm, b	Fresh scarp, open fissures in tundra	S	~83	N-up	Reed (1961), Plafker et al. (1994)
East Fork fault 2 (Southern)	Holocene	Qaa, Qai, b	Fresh scarp, open fissures in tundra	S	~83	N-up	Reed (1961), Plafker et al. (1994)
East Fork fault 2 Cont'd?	Holocene	Qaa, Qai, Qab, Qgm, Qaf, Qcf, b	Geomorphic lineation	S	>60	N-up	
McLeod Creek fault	Holocene	Qaa, Qai, Qgm, b, Tn	Fresh scarp, abrupt range front	SSE	25-45	SSE-up	
Peters Dome fault 1	Holocene	Qaa, Qai, Qab, Qcf, Tn	Long-term scarp uplifting Nenana Gravel	S	15-45	S-up	Bemis et al. (2012)
Peters Dome fault 2	Holocene	Qaa, Qai, Tn	Long-term scarp uplifting Nenana Gravel	N	15-45	N-up	
Peters Dome fault 3	Holocene	Qaa, Qai, Qab, Tn	Sharp Ridge	W	~90	RL	

Table 4.4: Summary of Quaternary Faults in the Mt. McKinley Restraining Bend (continued)

Fault name	Activity*	Offset units	Geomorphic expression	Dip Direction	Dip (°)#	Relative motion	Source+
Peters East fault	Holocene	Qaa, Qai, Qab, Qaf, Qcg, Qgm, b	Fresh scarp	SSW	15-45	SSW-up	
North Slippery Creek fault	Holocene	Qaa, Qai, Qab, Tn	Geomorphic lineation	SSE	15-45	SSE-up	

* Time period during which the most recent displacement of the fault is constrained.
# Dip values were estimated based on geomorphic expression and the mapped trace of the fault.
+ No source means that fault was from this study

4.2.1 East of Apex

Active faults east of the restraining bend apex illustrate a rapid shift from contractional faulting near the apex to extensional faulting eastward away from the bend. Neotectonic mapping to the east of the apex of the restraining bend and Peters Glacier shows a thrust fault following the north margin of the foothills. This thrust fault is called the Carlson Creek fault, which dips to the SE and flanks the northern edge of the foothills from Peters Glacier to Cache Creek (Figure 4.1). To the south of Carlson Creek fault, trending NW to SE along a similar striking ridge is the SSW dipping Peters East fault which offsets alluvial and moraine deposits. Evidence for active thrust faulting ends on the west side of Cache Creek and, in less than 2 km to the east across this drainage, evidence for active faulting is expressed as normal faults. These active normal faults, collectively referred to as the East Fork faults, demonstrate a consistent south side down sense of predominantly dip-slip displacement (Figure 4.7) that is continuous from Cache Creek eastward to the Muldrow Glacier.

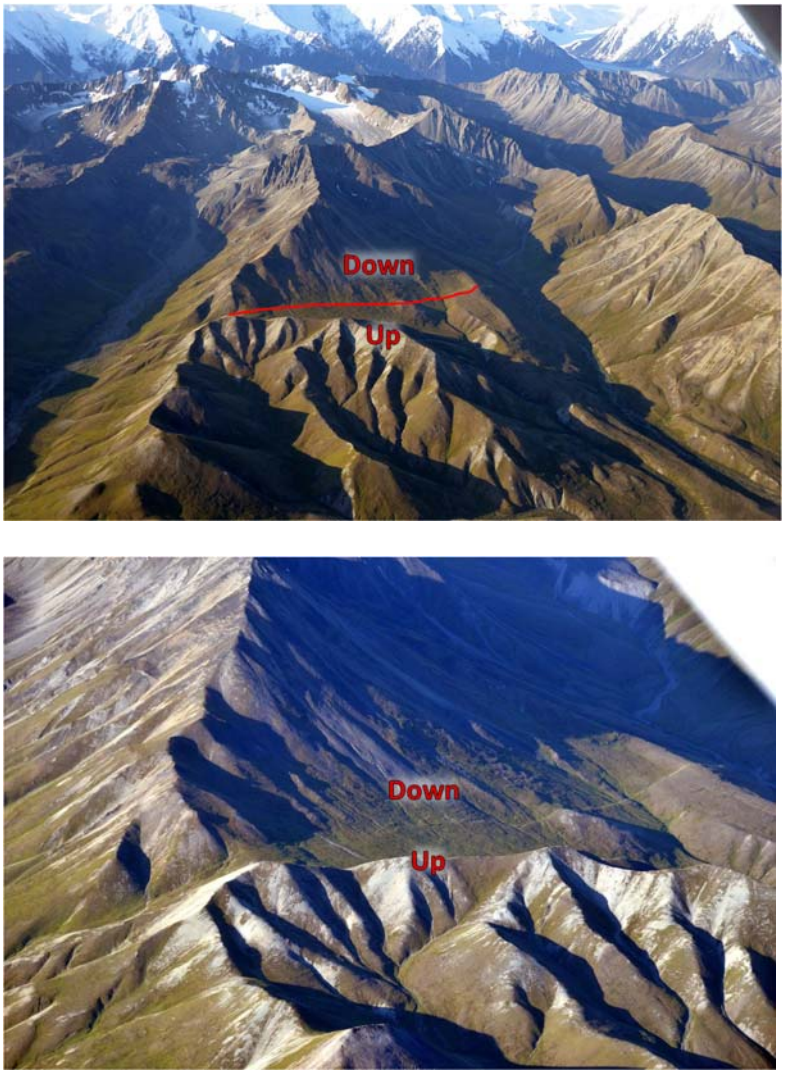

Figure 4.7: Southern East Fork fault. View to the southeast towards the Denali fault. The south-side down displacement shown in the image of the East Fork faults oppose the south-side-up topographic expression of the foothills. The bottom image is a zoomed in image of the fault and the fault can be seen clear by the offset shadow in the bedrock. The red line traces the fault trace. The down and up labels just show relative motion.

The map traces of the normal faults illustrate a fairly linear fault trace across topography, indicating a relatively steep fault dip. Where the scarp of the southern East Fork fault is well-preserved across a ridge (Figure 4.7), I used a 3-point problem to determine the fault has a steep, southeastward dip of 83 degrees. Although the scarp of the northern East Fork fault does not allow for a reliable 3-point problem calculation due to fault step-overs and transecting gentler topography, the linear trace does indicate that it is near vertical, probably with a slight southward dip. The normal displacements of the East Fork faults oppose the south-side-up topographic expression of the foothills. Even with the reconnaissance-scale of previous mapping (Reed, 1961; summarized and reinterpreted by Wilson et al. (1998) on Figure 1.3), the south-side-down motion across the East Fork faults are clearly not the long-term sense of displacement. I interpreted the northern East Fork fault (Figure 4.8; 4.9) to extend past Cache Creek to the Peters Glacier based on a geomorphic lineament seen in the digital elevation model. This same geomorphic lineament was included in the map by Reed (1961) as part of his main range bounding fault across the Peter Dome foothills.

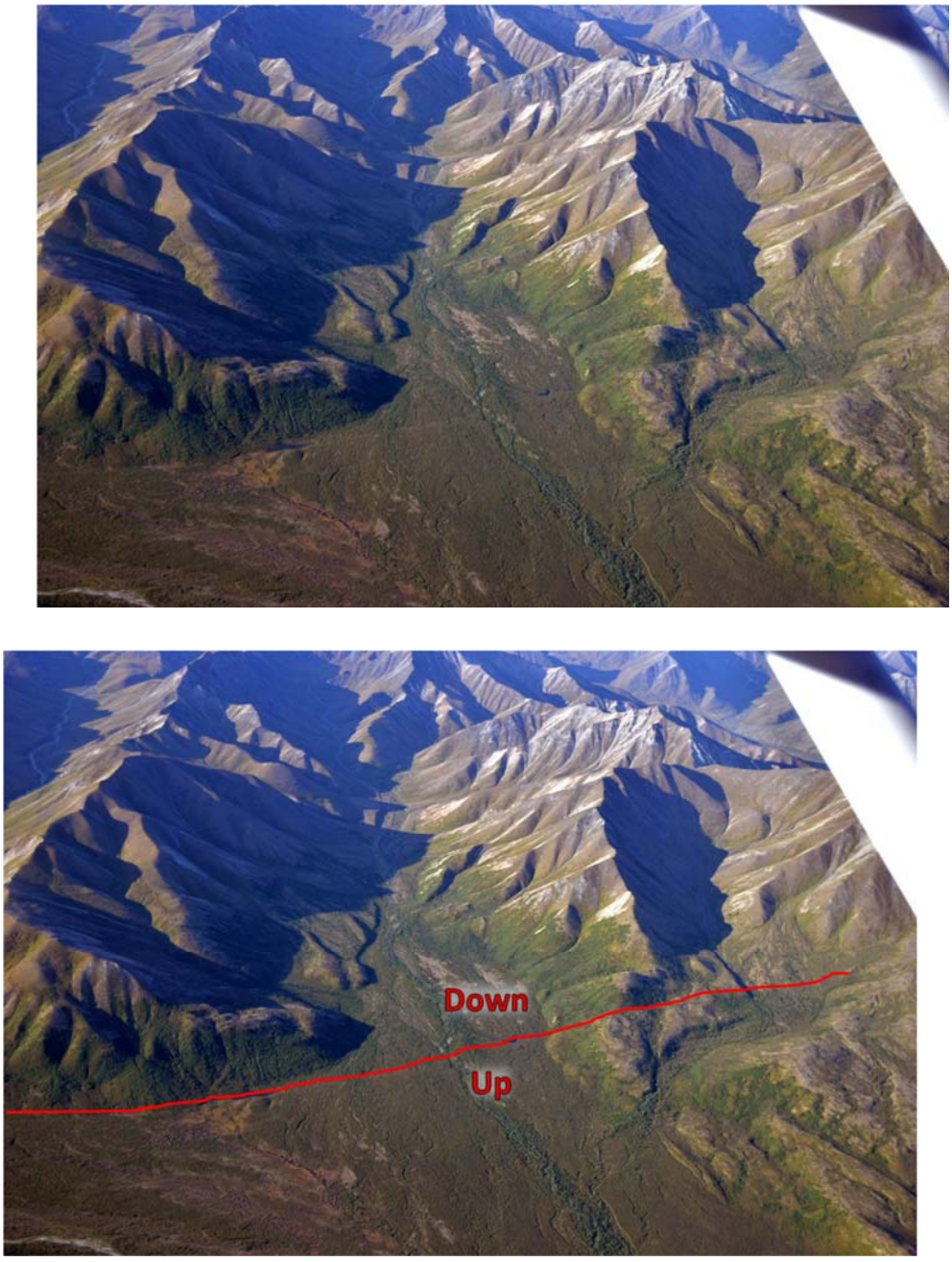

Figure 4.8: Northern East Fork fault. View to the southeast towards the Denali fault. The south-side down displacement shown in the image of the East Fork faults can be distinguished by the ponds forming along the fault trace. As the southern block moved down it created accommodation space allowing water to become ponded.

Figure 4.9: Northern East Fork fault looking southwest. This perpendicular view compared to Figure 4.8 showing the ponds in greater detail.

Previous mapping indicates that the bedrock geology also transitions abruptly west of Cache Creek with the Cantwell Formation being mapped to the north of the geomorphic trend of the northern East Fork fault (Figure 4.1), whereas the Nenana Gravel is mapped north of the northern East Fork fault to the east (Reed, 1961). Although geologic exposure is relatively poor for both of these mapped units north of the northern East Fork fault, the apparent juxtaposition of units across Cache Creek suggests either misidentification of units by previous mappers or the presence of a relatively young transverse structure. Although I was unable to review these unit designations in the field, the morphological expression and tonal characteristics expressed on DEMs and satellite imagery (respectively) support the interpretation that these are different units. A transverse fault within the Cache Creek drainage that juxtaposed the Cantwell Formation and Nenana Gravel may also help to accommodate the rapid east-west transition in faulting styles across Cache Creek.

4.2.2 West of Apex

West of the restraining bend apex the width of the Peters Dome foothills expands and is dominated by thrust fault-related deformation. On the western edge of the restraining bend, the south dipping Peters Dome fault 1 is the northwestern edge of the deformation front and flanks the largest Nenana Gravel surface plateau of the foothills (Figure 4.1). To the east, a north dipping back thrust parallels the Peters Dome fault 1 and is called Peters Dome fault 2. Along the edge of the plateau farther east there is a sharp break in slope as the deformation front of the foothills steps back towards the Denali fault. This sharp break is a transverse fault separating

the northwest displacement of the Peters Dome fault block relative to the Northern Slippery Creek fault block. I called this fault the Peters Dome fault 3 having endpoints at Peters Dome fault 2 and the Northern Slippery Creek fault that is inferred along the abrupt front of the foothills starting at the end of the Peters Dome fault 3. I inferred the SSE dipping Northern Slippery Creek fault across the Slippery Creek drainage to flank an adjacent Nenana Gravel plateau-like surface that lines up with the Nenana Gravel front to the west.

Deformation steps again towards Denali, nearing the apex of the restraining bend along the Denali fault. Here the range front is defined by two thrust faults the SE dipping Birch Creek fault and the SSE dipping McLeod Creek fault. The Birch Creek fault exists from the west fork of Slippery Creek to Straightaway Glacier with its best exposure seen around Birch Creek with a clear contact between the uplifted Nenana Gravel surface and the undifferentiated bedrock. This fault is not defined by fault scarp like a majority of the other faults. Instead, the fault was mapped along a contact between crystalline bedrock and Nenana Gravel that continues parallel to the Denali fault. The Birch Creek fault is a concealed fault when it crosses the surficial deposits of the Birch Creek drainage since its known on both sides of the drainage, but not expressed in the surficial deposits. To the north of the Birch Creek fault, starting at the eastern extent of the fault there is a geomorphic lineament separating Nenana Gravel from another sedimentary package. I have inferred a thrust fault along this trend based upon the topography being higher and more incised south of the trend.

4.2.3 Apex

I have assumed that the scarps associated with the main borderland fault near the eastern apex of the restraining bend would be a prime location to understand the kinematics of the restraining bend and to estimate the amount of strain being partition from the Denali fault by the Quaternary thrust faults. To accomplish this, the McLeod Creek fault and associated scarps were selected for a detailed analysis. The McLeod Creek fault is the main range-bounding thrust fault near the apex of the restraining bend that extends southwestward for about 13 km from the Peters Glacier to the west fork of Slippery Creek. There are two overlapping surface scarps at the McLeod Creek drainage and two more surface scarps are exposed across the Slippery Creek drainage. I collected topographic profiles across fault scarps in the McLeod and Slippery Creek drainages (Figure 4.5). The hanging wall and footwall of the scarps were well defined with minimal error from the hummocky terrain and regional slope and had a clear vertical offset, which will aid in more accurate slip rates.

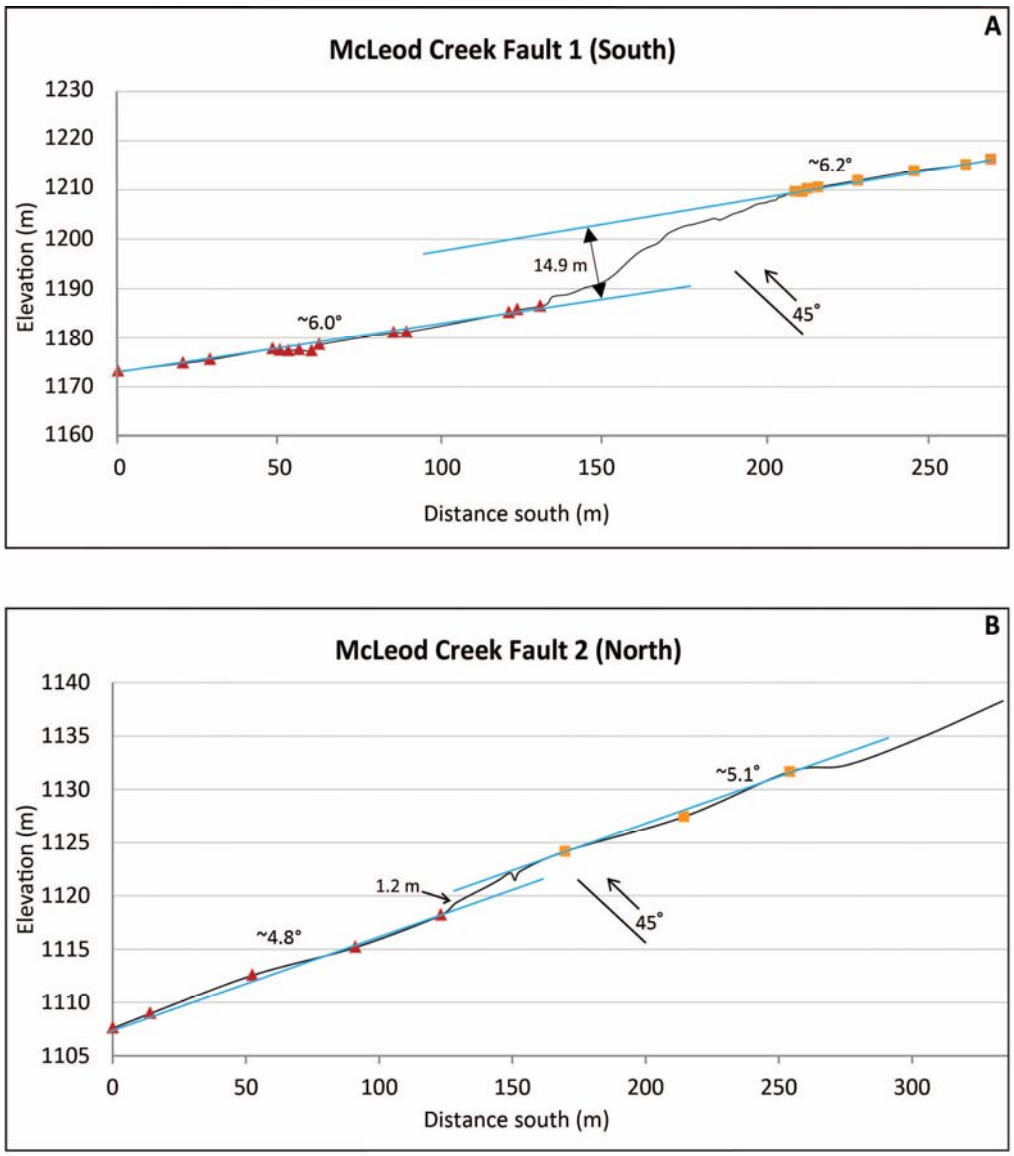

Figure 4.10: McLeod Creek topographic scarp profiles. A) North segment of McLeod Creek (Figure 4.2 (#1)) shows the largest vertical offset of any profile (14.9m). The large offset is assumed to be related to a higher seismicity rate or an irregular displacement cycle among this thrust system. B) South segment of McLeod Creek (Figure 4.2 (#2)) has the smallest vertical offset and seems to be a more recent exposure than the other scarp profiles. It is assumed that this scrap is evidence that the seismic stress is propagating outward away from the North segment, as the North segment becomes dormant and the South segment becomes more active. The hanging walls are orange square points while the footwalls are dark red triangles. Trends lines (light blue) are drawn for each hanging wall and footwall to calculate the average slope of each surface. The vertical offset is indicated by a double arrow line perpendicular to the trend lines, but this was not drawn for North segment because of small offset. Projected fault planes are placed in the subsurface.

The map-view image of the McLeod Creek scarps overlapping (Figure 4.5) suggests a fault stepover structure where the southern scarp becomes smaller east of McLeod Creek as the northern scarp becomes larger. A 45 degree dip was measured for the McLeod Creek fault from a large stream cut across the southern McLeod Creek fault strand, east of McLeod Creek, exposing a 45 degree SE-dipping fault plane. The scarps offset alluvium, glacial, and bedrock surfaces showing the potential maturity of the fault. (Table 4.4). I surveyed a topographic profiles perpendicular to each fault scarp which offset an alluvial surface. The southern scarp profile has a fault slip of 19.8 ± 2.3 m, while northern scarp profile only has a slip offset of 2.8 ± 3.7 m (Figure 4.10). These are two scarps across a surface of the same age, but with greatly different displacements of this surface. Clearly the southern scarp has experienced more earthquakes, and perhaps the northern one has developed more recently based on the morphology of this scarp seeming relatively young.

Figure 4.11: McLeod Creek scarps. A) An aerial view of the McLeod Creek scarps looking to the southwest. The black lines show the fault traces for each scarp. The red box indicates the zoom in view for the second image. B) This is a cross section view of McLeod Creek scarp 1 looking to the east. The elevated surface above the black fault trace is a moraine deposited and not an uplift surface by another fault.

The expression of the McLeod Creek fault in the Slippery Creek drainage consists of a 1 km continuous scarp across the east fork of the Slippery Creek drainage (Figure 4.12). I used the 3D expression of the fault scarp across a terrace riser to measure 25 degree SE dip. Similarly, the sinuous trace of the fault scarp as it traverses the ridge to the east suggests a relatively low dip angle. To document the displacement across this portion of the fault, I collected three topographic profiles across the scarp and use them to calculate fault slips of 4.2 ± 0.8 m (Slippery 1; Figure 4.13), 3.4 ± 3.6m (Slippery 2), and 9.9 ± 0.6m (Slippery 3) (Figure 4.5; Figure 4.14). The scarp offsets only Qaa, Qab, and Qdf units showing younger displacement compared to the scarps at McLeod Creek. The morphology of this scarp also seems relatively young like the northern McLeod creek scarp reflective of probably only one or two earthquakes. A summary of all faults along the Peter Dome foothills are shown in Table 4.4.

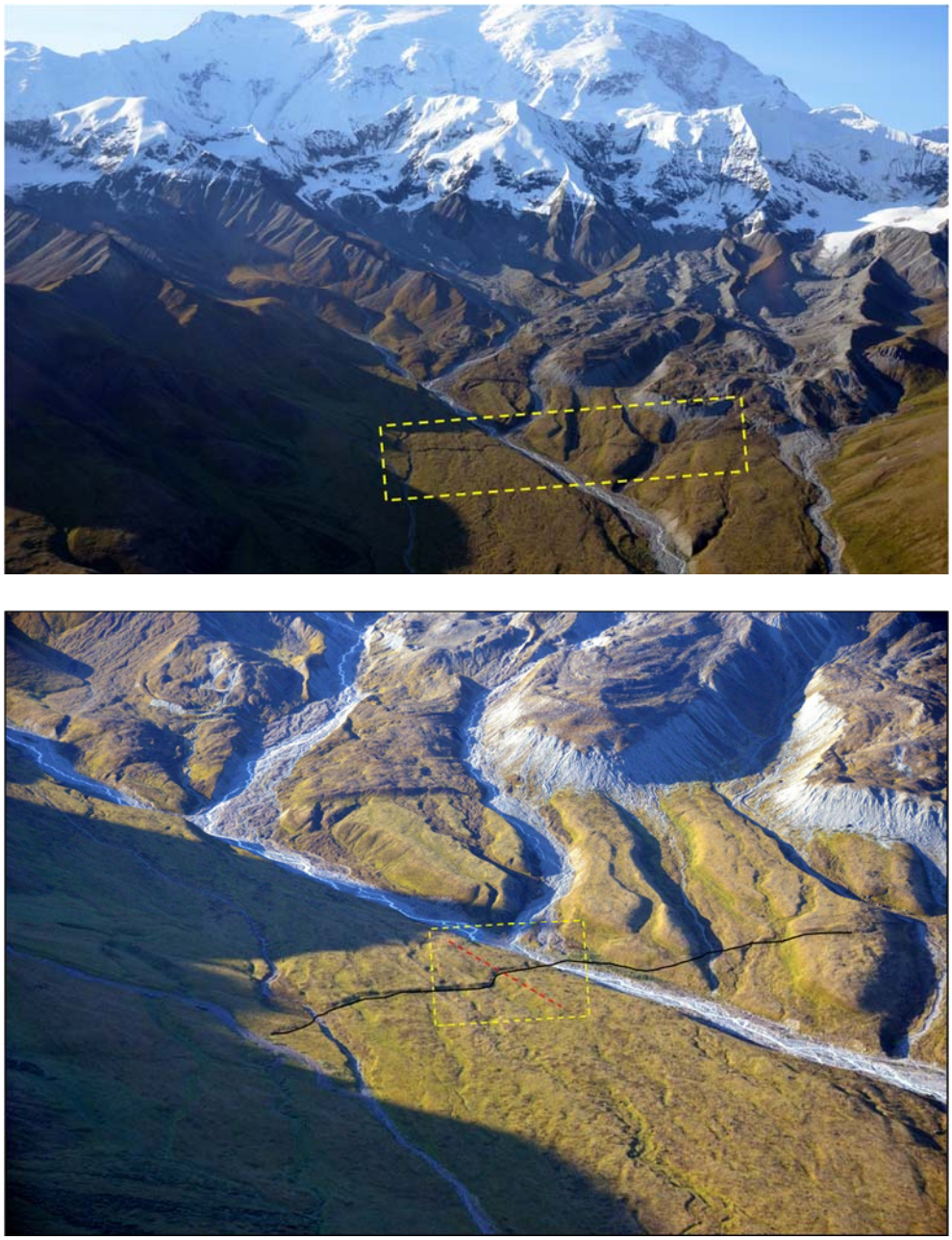

Figure 4.12: Slippery Creek scarp. A) An aerial view of the Slippery Creek drainage and the Slipper Creek scarp looking to the southeast. The scarp is offsetting alluvial and debris flow deposits. The yellow box defines the scope of the bottom image. B) This is a zoomed in version of the top image. Here the scarp is clearer in the offset surficial surfaces. The eastern portion of the scarp has a well-defined hanging wall and footwall surface. This portion of the scarp also has a discrete offset of the same surficial deposit making it a prime location for a topographic profile perpendicular to the fault trace to measure vertical offset. The red dash line is the profile line and the yellow dashed box indicates the area of Figure 4.13

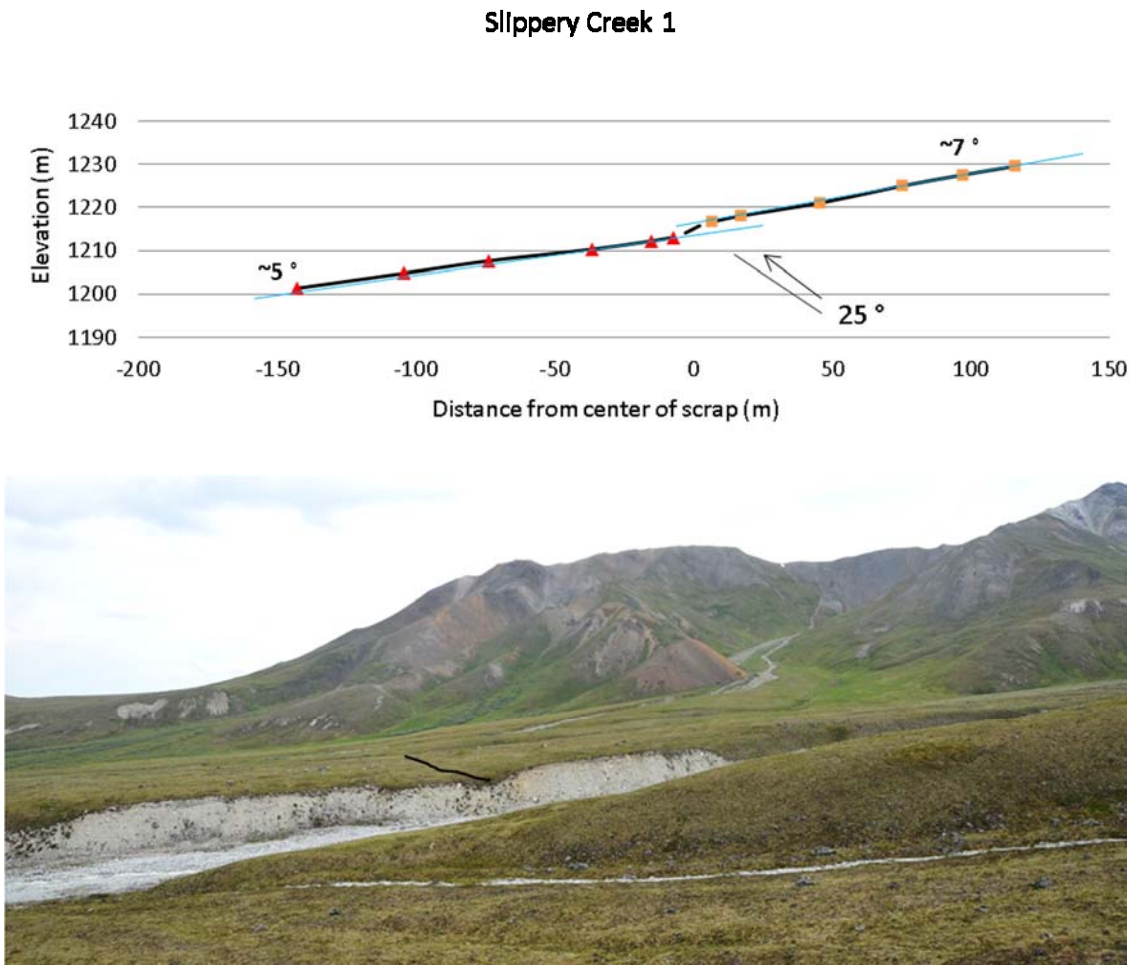

Figure 4.13: Slippery Creek topographic scarp profile one. The Slippery Creek 1 profile offsets a debris flow deposit. The west side of this deposit was cut on by the active east fork of Slippery Creek. In the subsurface, a continuous organic and clay rich layer group was discovered along western edge (buried soil) (Figure 4.6). This layer was folded by scarp deformation and offset at the base of the scarp.

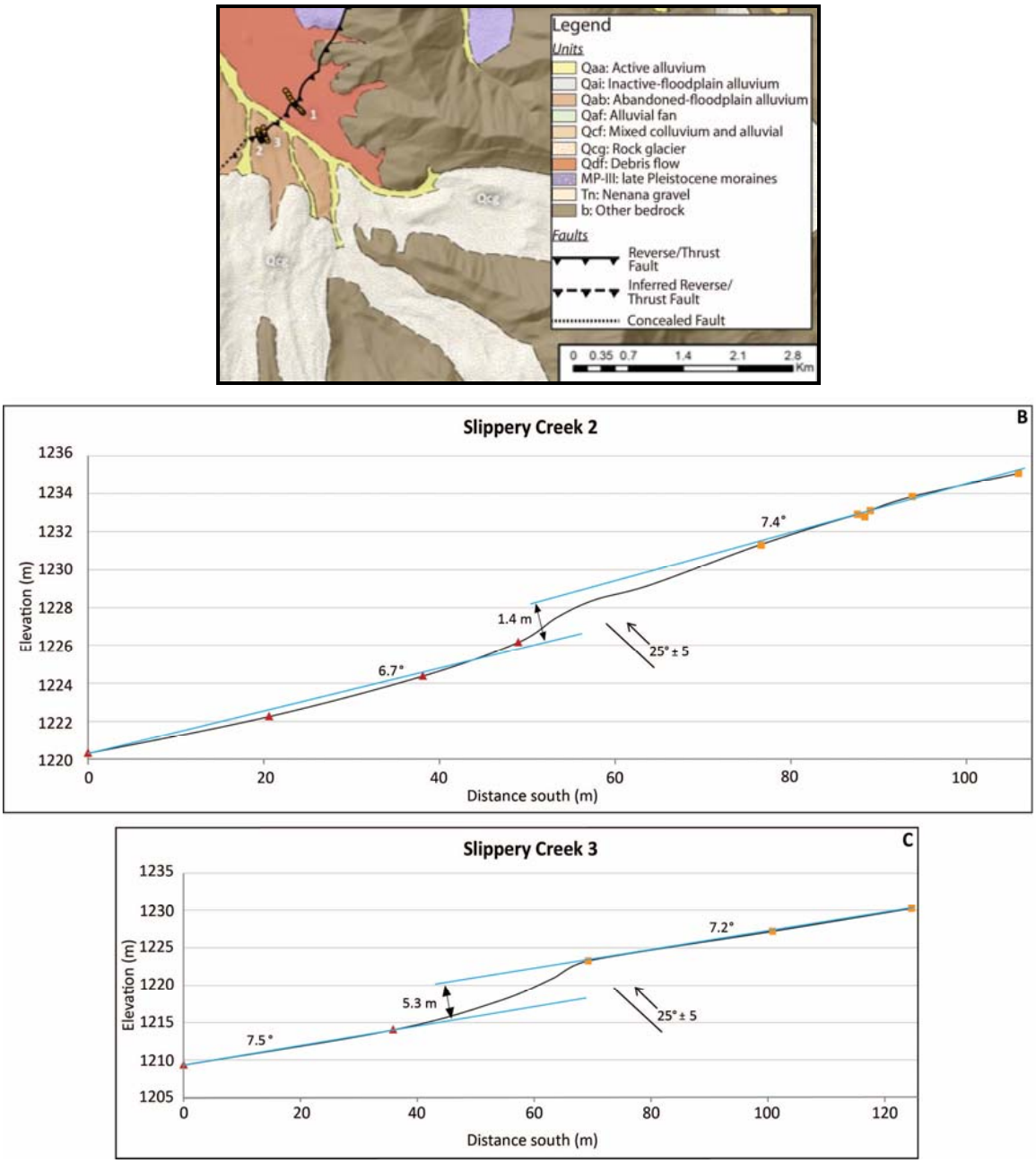

Figure 4.14: Slippery Creek topographic scarp profiles two and three. B) Slippery Creek 2 (Figure 4.5 (#2)) was on an abandon floodplain deposit that was cut on either side by active rivers. At depth a continuous organic and clay rich layer group was discovered along western edge (buried soil) (Figure 4.6). This layer was folded by scarp deformation and offset at the base of the scarp. C) Slippery Creek 3 (Figure 4.5 (#3)) surface was the same as Slippery Creek 2 and has the largest vertical offset of the 3 (5.3m). It is unclear if this measurement is inaccurate or not, since vertical offset changes significantly over a short distance.

4.2.3.1 Fault Slip Rates at Apex

The topographic profiles across the scarps of McLeod and Slippery Creek provided the necessary information to calculate fault slip rates along the McLeod Creek fault. Given the regression uncertainty and the meter-scale irregularities of the surveyed hanging wall and footwall surfaces of each scarp, slopes within a few degrees were assumed to be parallel. The surfaces do not have to be parallel, but non-parallel surfaces require specific equations and the slip cannot be estimated straight off the profile. The surveyed points of the topographic profiles define the hanging wall, the scarp face, and footwall of each scarp. I separated the points that delineate the hanging wall and footwall into their own data sets. Each data set undergoes a linear regression to establish trend lines through the survey points to define the equations representing the hanging wall ($y_h = m_h x + b_h$) and the footwall ($y_f = m_f x + b_f$). These equations give the necessary variables used in Thompson et al. (2002) vertical and slip offset equations (Figure 4.15). To calculate the fault slip for a particular scarp, first the vertical offset of the topographic surface is calculated by subtracting the y-intercepts of each fault wall block surface. For parallel surfaces, the vertical offset is

$$v = b_h - b_f \quad (1)$$

Next, using the vertical offset, the dip slip offset on the fault plane is calculated by

$$s = v\cos\alpha / \sin(\alpha+\delta) \quad (2)$$

where v is vertical separation, α is surface dip, δ is fault dip, and $\tan\alpha = m$. If the surface dip (α) of each fault wall block is not the same, then the two numbers are

averaged for the dip slip calculation. Fault slip rates are calculated by taking the fault dip slip (s) and dividing it by the age (a) of the fault surface obtained by one of the below dating methods.

$$\text{Slip Rate} = s/a \tag{3}$$

The dated glacial history of the Peter Dome foothills allowed me to constrain the maximum age window of the faulted surfaces and calculate minimum slip rates from those estimated ages. I further improved on the surface ages with radiocarbon data collect at Slippery Creek to calculate a maximum slip rate.

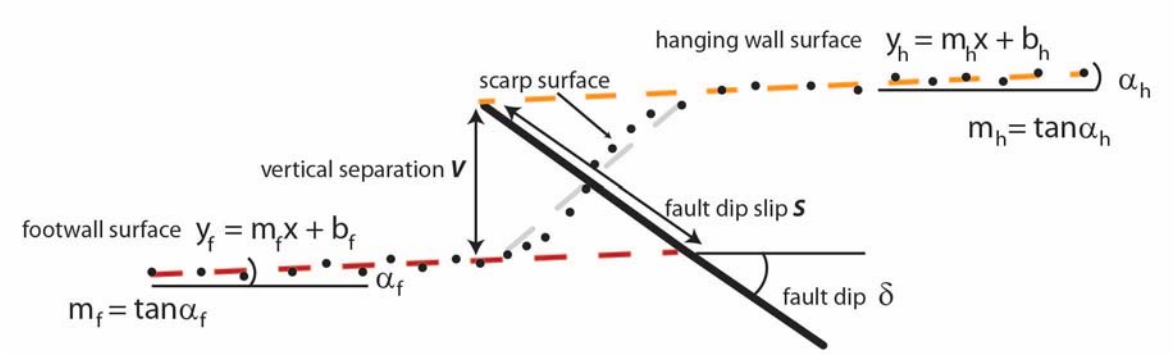

Figure 4.15: Fault scarp schematic for calculation of slip rates. Analysis of fault scarps adapted from Thompson et al., 2002. The black GPS points outline the geometry of the fault scarp. The dash lines are the trend lines that represent the hanging wall (orange)) and footwall (red) surfaces and are define by linear equations. The solid black diagonal line represents the fault plane with **S** being the fault's dip slip and **δ** being the fault's dip. Surface dip = **α**, vertical separation = **V**, footwall = **f,** and hanging wall = **h**.

Measurements of slip across the McLeod Creek fault were calculated from fault scarps preserved within the McLeod and Slippery creek drainages. The biggest uncertainty associated with these slip rate calculations is the age of the surfaces that

were offset. The absolute minimum slip rates are calculated by dividing the slip along the fault plane at each scarp profile by 12000ka for a Holocene age surface, resulting in slip rates of 1.7 ± 0.2 mm/yr (McLeod 1), 0.2 ± 0.3 mm/yr (McLeod 2), 0.3 ± 0.3 mm/yr (Slippery 2), and 0.8 ± 0.05 mm/yr (Slippery 3). The maximum slip rates were calculated by dividing the fault plane along the Slipper Creek scarp slip by 630 BP from the wood radiocarbon ages, resulting in slip rates of 6.5 ± 6.9 mm/yr (Slippery 2), and 19 ± 1.1 mm/yr (Slippery 3) based on the radiocarbon samples. It has to be noted though that a slip rate for these assumed to be one or two event scarps is highly uncertain because I am not necessarily seeing a complete earthquake cycle or how well the earthquake cycle would represent the long-term slip rate.

The slip rate errors were estimated using a resampling approach called the bootstrap method. A bootstrap sample of each profile of elevation (y) data was collected in R statistical software, where a resampling of the elevations that define the hanging wall and footwall is completed to delineate 50 different elevation samples for each profile. Each sample of the 50 was then used to calculate the Simple Linear Regression slope and y-intercept coefficients. These coefficients were then used to compute my estimate on the amount of fault slip on the fault plane. Then, assuming that the bootstrap sample estimate distribution would be approximately normally distributed we calculated the standard deviation and mean of the bootstrap estimates to obtain the estimate and standard error. Because little is known about the statistical distribution of the estimates and the sample set was small, we could not use traditional methods to approximate the standard error.

These fault slip rates define the rate of slip on the surface faults, but to relate these slip rates on thrust faults to strike-slip deformation on the Denali fault I can convert these slip rates into horizontal shortening rates. These rates define limits on the amount of contraction across the Peter Dome foothills and parallel to the left stepping portion of the restraining bend. Considering that contraction across this system is driven MMRB-related deformation from the south, this relative horizontal motion across these thrust faults to the northwest should be equivalent to the rates of horizontal motion of the trace of the Denali fault. The absolute minimum shortening rates that is accommodated by the faults north of the Denali fault are 1.2 ± 0.13 mm/yr (McLeod 1), 0.2 ± 0.2 mm/yr (McLeod 2), 0.3 ± 0.3 mm/yr (Slippery 2), and 0.8 ± 0.1 mm/yr (Slippery 3).

4.3 Seismicity

4.3.1 Regional Seismicity

Seismicity associated with the Kantishna Cluster covers an irregularly shaped region extending to the north and northwest of the area west of the eastern apex of the MMRB overlapping the active thrust faults. A minimal amount of seismicity exists to the east of the apex around the East Fork faults. The persistent low-magnitude seismicity has exhibited earthquake rates much higher than regional background seismicity rates for the duration of regional seismic monitoring, with over 18,000 earthquakes (of magnitudes ranging from <1 to 5.2) in the last 48 years.

Detailed analysis of the Kantishna Cluster identified 3 primary subzones of seismicity: the north, middle, and south zones, distinguished by lineations in the cluster and their orientation to the Denali fault (Figure 4.16; Ruppert et al., 2008; Burris, 2007). The orientation of the each seismic zone to the principle NW-SE stress has led to different kinds of strain seen in their focal mechanisms and the treads in the focal mechanisms (Figure 4.17). I characterized the zones to provide a more detailed analysis on the local structure and strain in each zone. The north zone strikes in a SW-NE direction and is characterized by right lateral and thrust slip in the NE with the majority of thrust/reverse slip focal mechanisms to the SW being oblique following the Cronin (2010) classification based on the rake of focal mechanism. The majority of the FMs in the Kantishna Cluster show that the majority of slip occurs in reverse/thrust slip clusters separated by right lateral fault zones as shown by the distinct trends in the middle zone. The middle zone strikes in an east-west direction with a slight curve in the mapview of the epicenters and has two major right lateral strike-slip trends cutting through the zone defined by focal mechanisms (Figure 4.18). The south zone strikes in a NNE-SSW direction. The right-lateral slip focal mechanisms of the south zone are parallel to the Denali fault to the southwest as the northeast right-lateral slip focal mechanisms are still near perpendicular to the Denali fault (Figure 4.19). These focal mechanisms with a right lateral strike slip component rotate 90 degrees when going from NE to SW in the south zone.

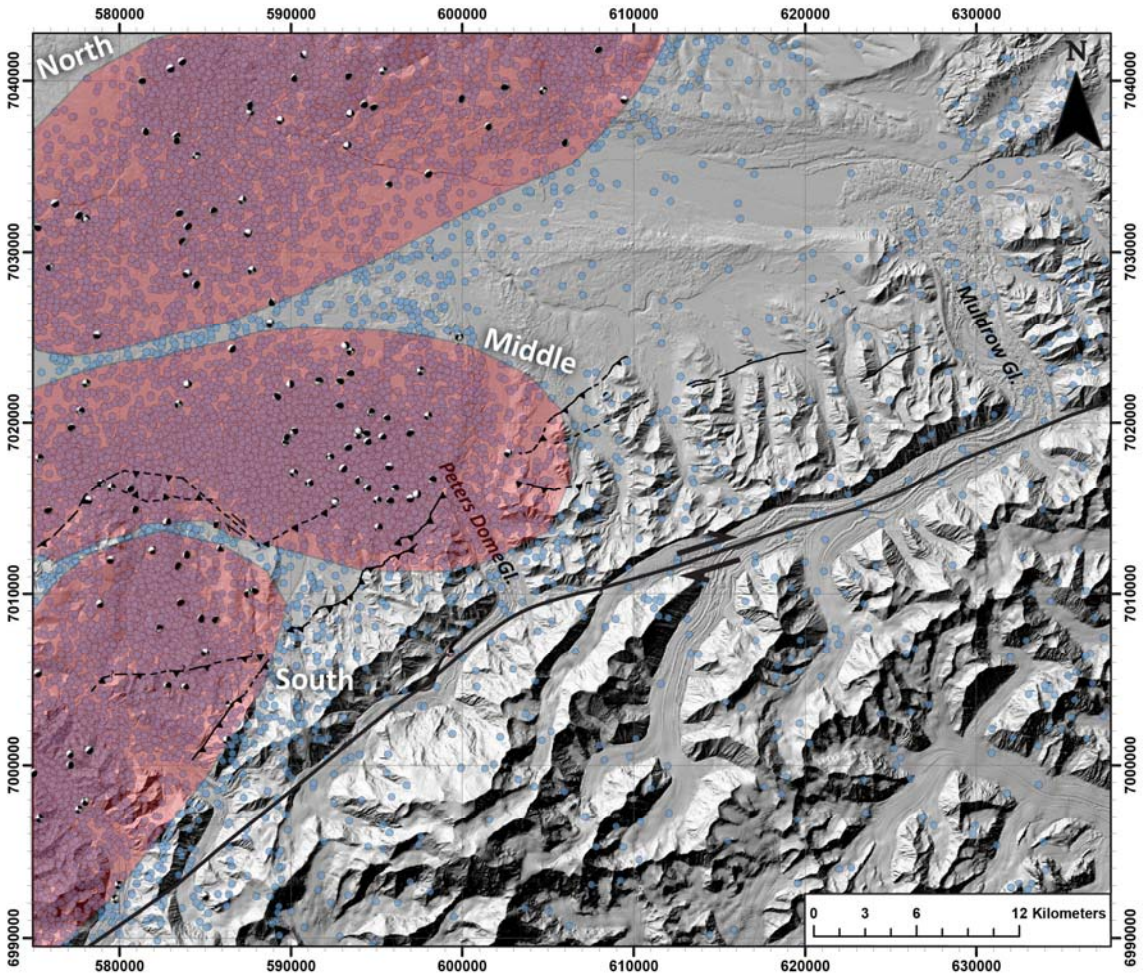

Figure 4.16: Quaternary faults overlain on Kantishna Cluster seismicity. The active faults are clustered over the active seismicity with the majority of the focal mechanisms seen in the zones being thrust/reverse slip focal mechanisms.

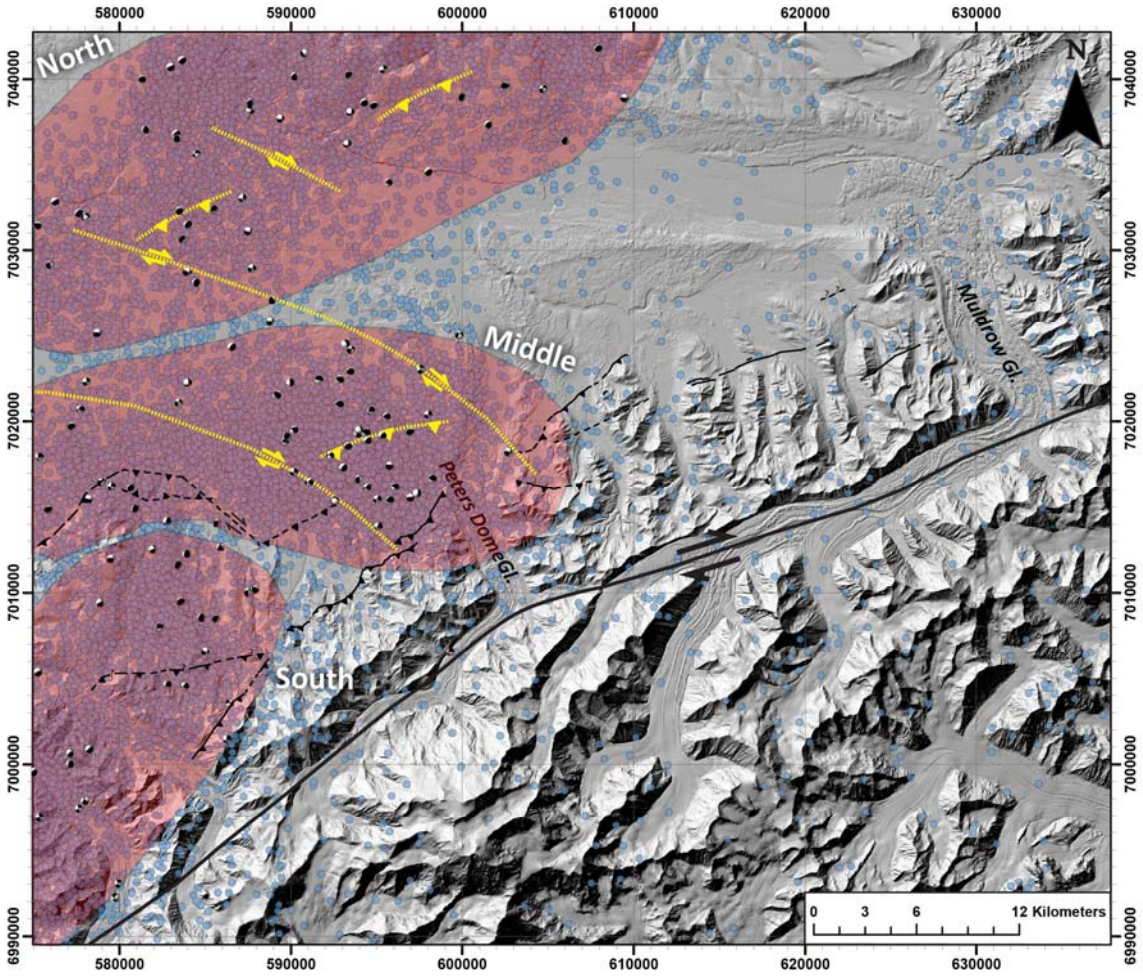

Figure 4.17: Seismicity trends north of the Mount McKinley restraining bend. The focal mechanisms of the zones define multiple trends through the Kantishna Cluster. Two right-lateral strike-slip trends parallel each other and curve from SE to NW through the middle seismic zone. The focal mechanisms show oblique to pure reverse/thrust motion between the strike-slip trends accommodating their motion. The north zone shows a continuation of the eastern from the middle zone as well as a smaller right-lateral strike-slip trend to the east. These two strike-slip trends in the north zone of also accommodated by reverse/thrust slip focal mechanisms.

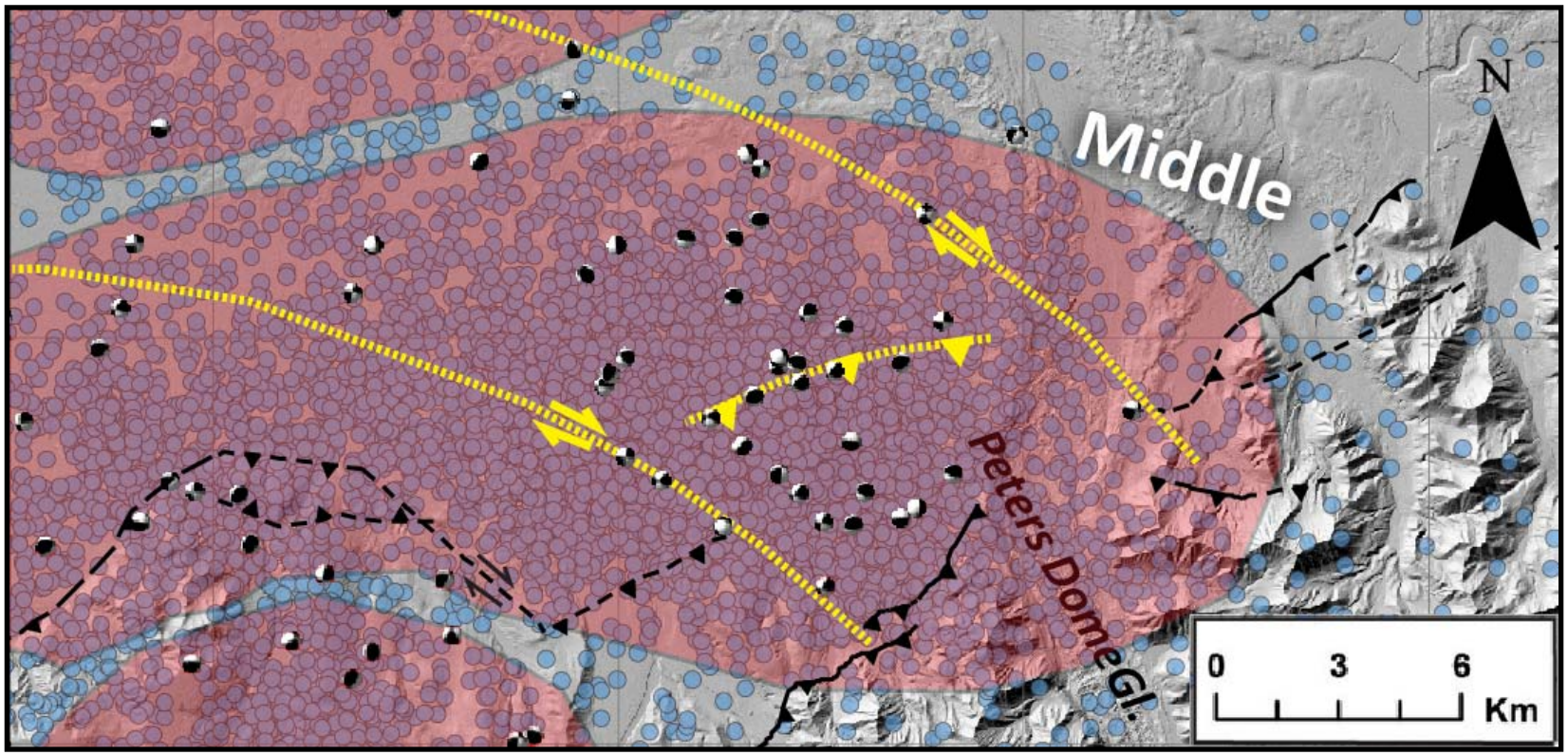

Figure 4.18: Seismicity of the Kantishna Cluster middle zone. The middle zone strikes in an east-west direction with a slight curve to the seismicity trend. This zone has two major, parallel right lateral-trends defined by focal mechanisms that strike SE to NW. The focal mechanisms show oblique to pure shortening displacement separating the strike-slip trends. The changes along strike of the thrust faults correspond with the trends in the background seismicity. The yellow dashed lines represent the seismic trends according to the focal mechanisms.

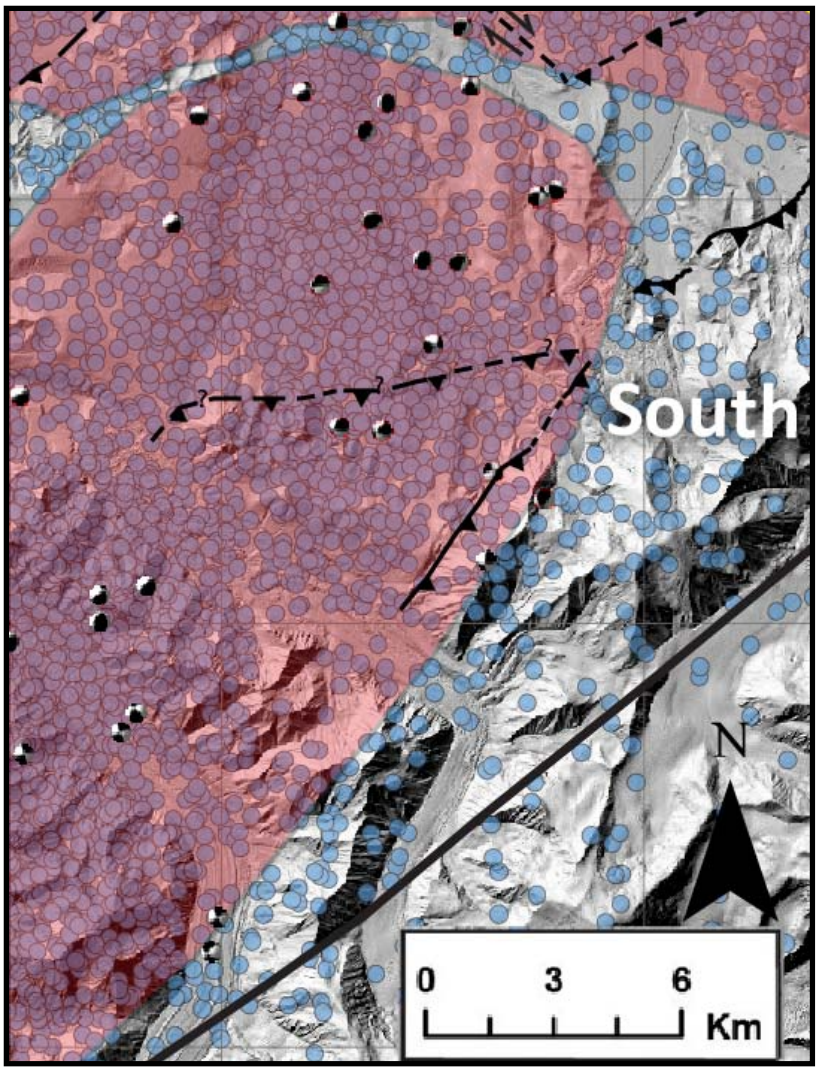

Figure 4.19: Seismicity of the Kantishna Cluster south zone. The south zone strikes in a NNE-SSW direction and is mainly thrust faults. The FMs show parallel right lateral strike slip strain to the southwest as the northeast FMs are still near perpendicular to the DF. This means that the FMs with a right lateral strike slip component have rotated 90 degrees going from NE to SW in this zone

4.3.2 Seismicity Trends

Focal mechanisms of the cluster were used to search for trends in the seismicity that might represent active faults that are not clearly expressed at the surface. The visual analysis of seismicity trends highlighted prominent focal mechanisms, lineaments of seismicity, and showed how earthquakes lined up with the known faults. Two right-lateral strike-slip trends, defined by 6 focal mechanisms each, are parallel and curve from SE to NW through the middle seismic zone (Figure 4.18). The FMs show oblique to pure reverse/thrust motion between the strike-slip trends accommodating their motion. The surface evidence for these trends are the jogging of rivers at right angles to the west and along strike faulting changes corresponding to the trends. For example, the northern Slippery Creek fault ends abruptly at the west strike-slip trend and the McLeod Creek fault 3 ends suddenly at the east strike-slip trend. Other right-lateral and reverse/thrust trends exist in the north zone, but the SW trend of the north zone is a continuation from the middle zone's eastern trend.

These strike-slip trends encompass the higher magnitude earthquakes seen in the Kantishna cluster, remembering that a 5.2 magnitude earthquake is the maximum recorded in the cluster (Ruppert, et al, 2008). The major focal mechanisms of the eastern trend range in magnitude from 3.5 to 3.7 occurring from 1991 to 2003. While the major focal mechanisms of the western trend range in magnitude from 4.1 to 4.8 occurring from 1993 to 2013. The magnitude of the focal mechanisms on average increases to the west when comparing the parallel SE to SW right-lateral trends. This portrays a relationship between the location of each trend

and the average magnitude, which could be related to active deformation west of the eastern apex.

4.3.3 Subsurface Structure

The lack of geomorphic signatures related to the seismic trends at the surface supports that these focal mechanisms at depth correlate to subsurface structures. Also the seismicity suggests the need for more active structures to accommodate the Kantishna Cluster, especially in the middle and north zones where there is a lack of surface Quaternary faults. The idea of subsurface structures was tested by viewing the focal mechanisms at depth below the Peter Dome foothills in ArcScene. The cluster of focal mechanisms at depth appears as an almost random cluster of earthquakes with some minor subzones similar to the zones at the surface. The limitations of the ArcScene software does not allow sufficient zoom from any angle, making it hard to characterize the subzones.

Rather, I plotted the X, Y, and Z coordinates of each hypocenter in ArcMap and overlaid the hypocenters on a digital elevation model. This allowed me to take cross sections through the Kantishna Cluster with the point profile tool. In particular I focused on subsurface structure the middle and south zones since these are in the restraining bend deformation extent. With the zones having a elliptical shape, one cross section was taken along the long axis. Then another cross section was taken perpendicular through the portions of each zone that had a high density of hypocenters. The goal of these cross sections is to image the structure of the middle and south zones at depth. Spatial location errors exist horizontally and vertically for

each hypocenter and this uncertainty makes detailed analysis of fault planes and seismic trends difficult, but relative observations can still be made.

The first set of cross sections were taken of all 18,000 plus hypocenters that were recorded from 1986 to 2013 (Figure 4.20). Cross section A to A' appears to show the cluster bending at the same bend seen in the mapview of the middle zone suggesting multiple structures. After bisecting that transect with a perpendicular cross section (Ax-Ax'), no planar structures are imaged, but the hypocenters have a north dipping subsurface trend. This north dipping trend correlates with the thrust/reverse slip mapview trend through the middle cluster zone, in which the focal mechanisms get deeper to the north. The hypocenter locations of the south zone to the southwest show increase in seismicity to the northeast of the zone along the B-B' cross section. The increase in seismicity is imaged in the Bx-Bx' cross section by bisecting the B-B' cross section perpendicularly. Just like the middle zone, the diffuse seismicity does not clearly define individual structures.

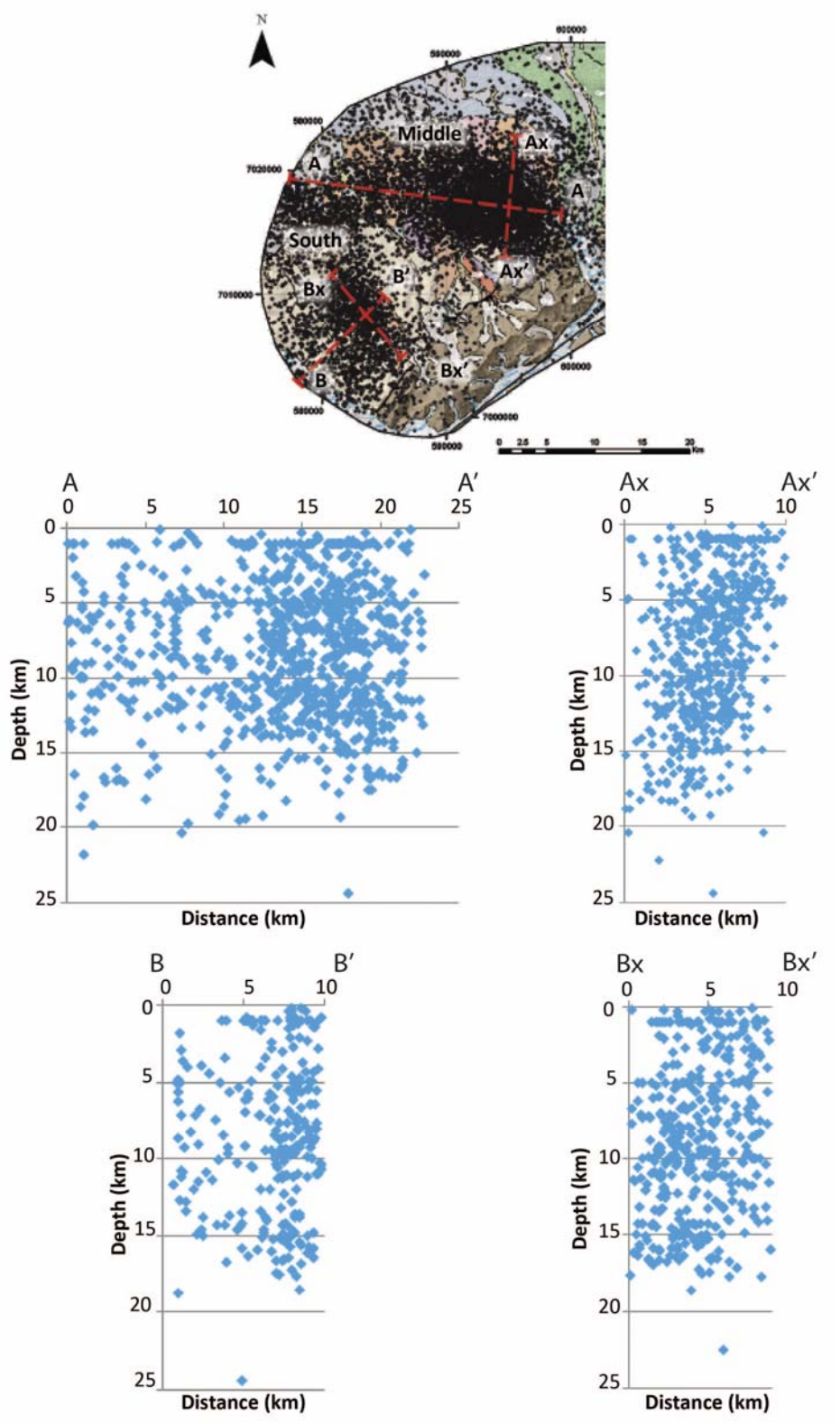

Figure 4.20 Cross sections of middle and south zones. These show the middle and south seismic zones character at depth when earthquake events are projected at depth. The red dotted lines show the locations of the cross sections.

On the contrary, if the diffuse seismicity is a product of noisy data, then perhaps sorting the hypocenter data to analyze only earthquakes with higher location precisions would better highlight subsurface faults. I used a total of four parameters. Hypocenters with an average horizontal and vertical error less than 1 km were used in view of trying to image structures on the order of 5 to 10 km. Also all hypocenters after 1989 since two local stations were installed in 1988 and 1989 (Ruppert et al, 2008), and all hypocenters after 2005 considering the last of six broadband sensors were installed in 2006 (Ruppert et al, 2008). Finally only hypocenters greater than a magnitude of 2 were used, after seeing that the locations errors decrease overall for hypocenters that have magnitudes greater than 2. However the cross sections again showed diffuse seismicity with no defined structure (Figure 4.21), but the hypocenters of the Cx-Cx' and Dx-Dx' cross sections have a north dipping subsurface trend like the Bx-Bx' cross section. Again, the diffuse deformation makes it hard to say if there is a true north dipping structure or if this is even a single structure, but it does show the complexity of the Kantishna Cluster and its associated subsurface structure.

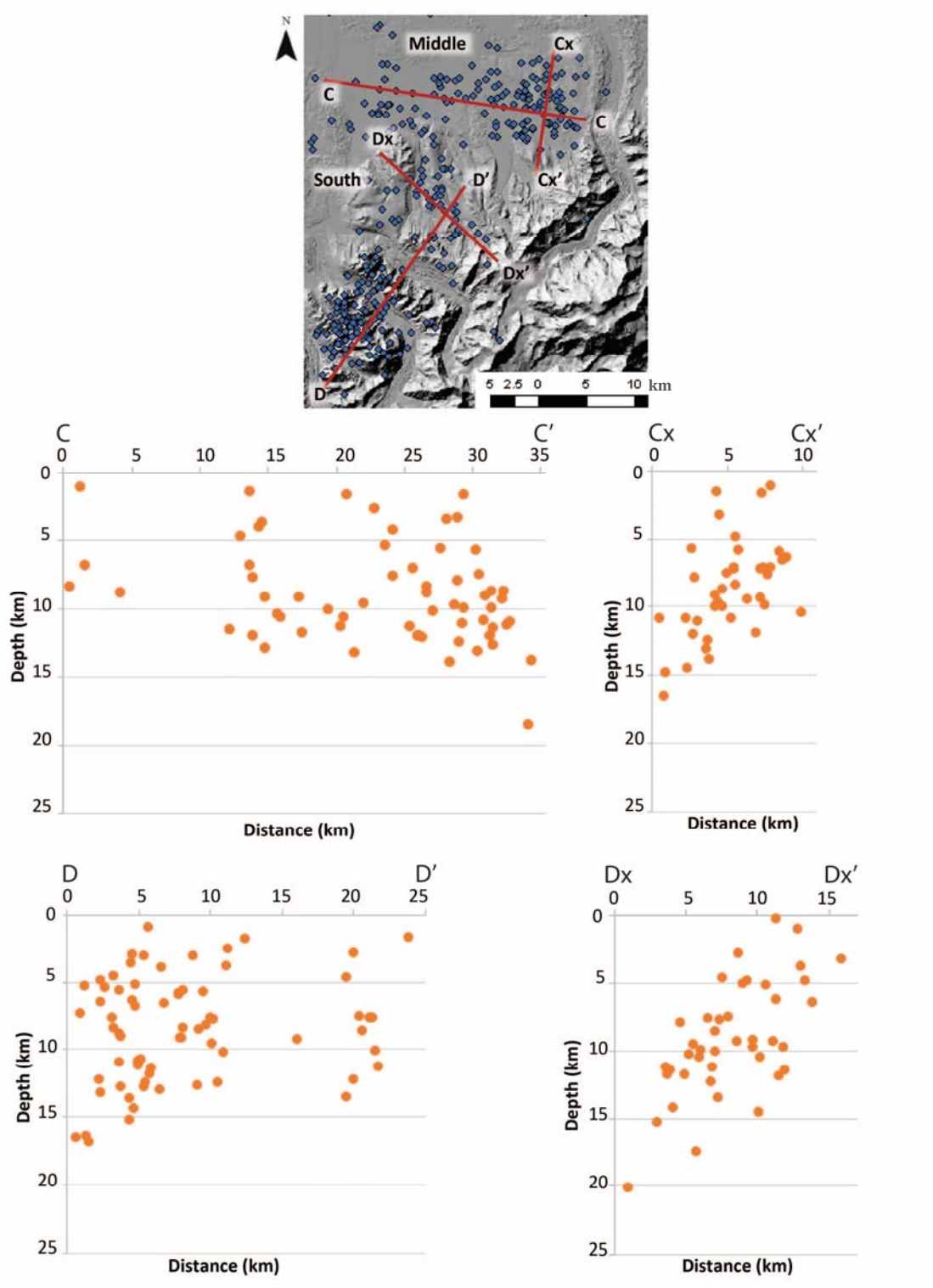

Figure 4.21 Cross sections of middle and south zones without noise. A filter set of hypocenter were compiled based on 4 parameters discussed in detail in the text above to eliminate the noise of the dataset to better image structure. The red dotted lines show the locations of the cross sections.

CHAPTER FIVE: INTERPRETATION AND DISCUSSION

The Denali fault has developed over millions of years and is a mature fault zone. Despite the relatively long-lived Denali fault trace and structural maturity, several bends have formed that result in significant deviations from the regional small-circle arcuate fault trace of the Denali fault (e.g., Stout and Chase, 1980). For the most part, the geometry of these bends increases the component of contraction across the system, making these restraining bends produce concentrated shortening adjacent to the Denali fault in order to accommodate lateral crustal movement past the bend. The 17 degree eastern bend in this system is associated with the greatest topographic development in the Alaska Range and formed asymmetrically relative to the Denali fault. Numerical modeling of restraining bends in wet kaolin clay show bends that are < 20° will naturally exhibit asymmetric topography (Cooke et al., 2013). This shows the strong structural control the restraining bend has on orogenic development along its segment of the Denali fault.

The MMRB structure on the north side of the Denali fault consists of right stepping thrust faults that are generally parallel to the Denali fault and propagating to the northwest of the bend. Conversely, the structure south of MMRB is characterized by parallel thrust faults to the left stepping portion of this Denali fault bend and oblique to the Denali fault to the east and west of the restraining bend (Figure 1.2). The geomorphic preservation of these structures north of the Denali fault allowed me to complete this systematic study to achieve a first order understanding of the active deformation and evolution of the Mount McKinley restraining bend.

Now since I have presented the Quaternary geology, the structural geology and seismicity of the MMRB I will answer the questions I stated at the beginning. The questions were: 1) Is there a change in faulting style across the apex of the restraining bend that corresponds with the increase obliquity of motion to the northwest?, 2) Does a spatial relationship exist between the distribution of earthquake events and the locations of faults across the apex?, 3) How much of the slip budget for the MMRB system is accommodated by faults north of the Denali fault, 4) How is the Mount McKinley restraining bend evolving?.

1) Is there a change in faulting style across the apex of the restraining bend that corresponds with the increase obliquity of motion to the northwest?

My mapping documents an abrupt transition in subsidiary faulting styles where the southeast-dipping thrust faults to the west transition into East Fork normal faults to the east of Cache Creek. Satellite imagery and high-resolution topography do not exhibit evidence for recent fault scarps exhibiting similar displacement as the East Fork faults to the west of the apex of the MMRB. The south-side down normal displacement of the East Fork faults exhibits a change in the local stress field across the eastern apex of the restraining bend. The local stress field changes abruptly to accommodate this transition in the stresses driving active faulting from a vertical maximum principal stress allowing for extension and normal faults to a horizontal maximum principal stress associated with the thrust faults. There is evidence along the San Andreas fault in the borderlands (e.g., Legg et al., 2007), where local stress has rotated, in which, σ_1 is closer to perpendicular to the master fault plane. This differs from the oblique regional σ_1 stress orientation

(Mount and Suppe, 1987), allowing for the thrust dominated bends and fold and thrust belts seen in these locations of the San Andreas fault.

Focusing in on the longer, northern trace of the East Fork faults, the bedrock geology shows a south-side up relationship across the previously mapped fault trace (Reed, 1961), whereas the late Quaternary displacement clearly shows an opposite sense of slip shown by the geomorphic surfaces offset across the scarp. At 83 degrees, the dip of the fault exhibits minor extensional displacement. The East Fork faults could be reactivated strike-slip remnants of an older trace of the Denali fault before the fault was defined along a narrower zone of displacement similar to other major strike slip faults (e.g. Wesnousky, 1988) or the faults are older thrust faults that previously uplifted the foothills around the East Fork faults. Other possible scenarios exist, but based on the current evidence these seem to be the most popular. The East fork faults not flanking the foothills and having near vertical dips supports older Denali fault traces, but being major topographic faults, offsetting Nenana Gravel deposits supports reactivated older thrust faults.

2) Does a spatial relationship exist between the distribution of earthquake events and the location of faults across the apex?

Faults correlate with the active seismicity, but the majority of the active faults exist within the Kantishna Cluster to the west of the eastern apex. The transition in faulting styles across the apex also corresponds with a boundary between a region with abundant shallow crustal seismicity to the west overlapping the active deformation and minimal seismicity to the east of the apex with no

shortening. This distribution in seismicity supports some sort of change in local stress field to accommodate the pattern.

Examples of how the seismicity supports this change in stress orientation is 1) with the middle seismic zone of the Kantishna Cluster abruptly tapering out at Cache Creek transition boundary (Figure 4.16) and 2) the lack of seismicity to the east of the apex. The abundant seismicity of the Kantishna cluster is not accommodate by known surface faults, but my hypocenter cross sections support subsurface structure that could account for the rest of the seismicity. Although there are no definitive conclusions on the deeper structural geometry of these faults in this restraining bend, general models of restraining bends typically consist of faults having a convex-up fault geometry. These convex-up faults commonly transition from relatively shallow dips near the surface to steep dips as the fault approaches the primary strike-slip fault at depth (e.g. Harding, 1985).

Three factors seem to be main controlling factors on the seismicity and its trends in focal mechanisms. First, the diffuse seismicity at depth are related to a young fault zone, in which, overtime will define its seismicity along narrower zones, defining major fault planes. Next the trends in focal mechanisms might not produce surface ruptures because the earthquakes in the Kantishna Cluster do not seem to be at a high enough magnitude to produce a surface rupture. There has to be a magnitude threshold for earthquakes to create a surface rupture in any given location, but this failure threshold would be so site or fault specific as to render it nearly impossible to generalize a magnitude threshold for surface ruptures. Normally higher magnitudes are related to deeper hypocenters since an increase in

depth would increase the overburden stresses and allowing the needed loading to allow for failure. Finally the rheology of the crust is a main controlling factor on the seismicity. The diffuse seismicity seems to be linked to the weak, fractured metamorphic rock that makes up the majority of the Peter Dome foothills. This is compared to the rigid pluton block of Mount McKinley which lacks seismicity and has fault concentrated in between the plutons in the weaker “flysch” material. The rigid pluton block of Mount McKinley is rock uplift as one block contributing to the lack of seismicity compare to north of the Denali fault (Figure 5.1).

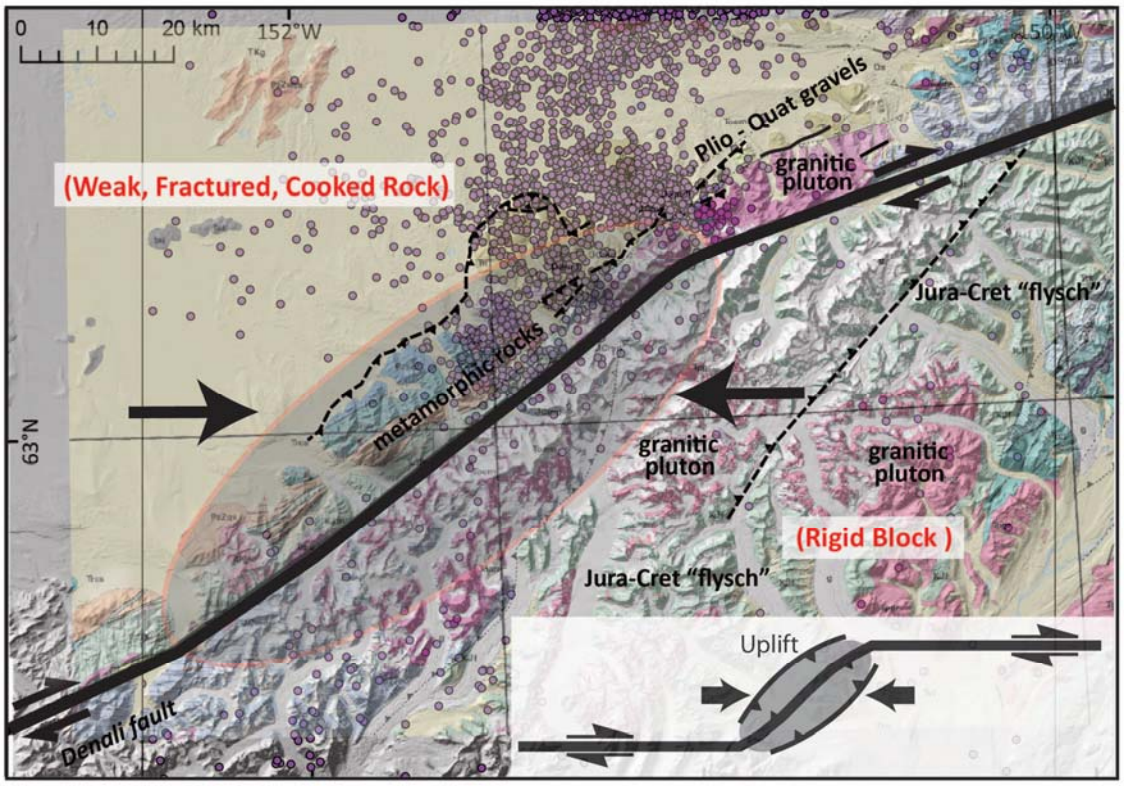

Figure 5.1: MMRB kinematic diagram. The Mount McKinley restraining bend of the Denali fault has a clear spatial relationship of active thrust faults along the restraining bend with the majority of shortening occurring all the oblique portion of the restraining bend. The Kantishna Cluster is concentrated along the eastern apex. The diffuse seismicity seems to be linked to the weak, fractured metamorphic rock that makes up the majority of the Peter Dome foothills. This is compared to the rigid pluton block of Mount McKinley which lacks seismicity and has fault concentrated in between the plutons in the weaker "flysch" material. The black inward-pointing arrows illustrate the oval region of Denali fault undergoing shortening.

3) How much of the slip budget for the MMRB system is accommodated by faults north of the Denali fault?

Shortening is occurring at and to the west of the eastern apex. To the east of the apex there is no neotectonic evidence for near-field late Quaternary shortening. The lateral slip rate on the Denali fault decreases after it goes through the Mount McKinley restraining bend (Haeussler et al, 2012). The slip rate is partitioned into the deformation occurring along the oblique portion of the restraining bend. Through my analysis I was able to determine the amount of slip accommodated by the McLeod Creek fault, which is the major fault north of the eastern apex. I calculated the McLeod Creek fault slip rate on multiple scarps along its trace. These fault slip rates define the displacement on a given fault plane, and for transverse thrust faults the horizontal component of this slip describes the map-view displacement of the hanging wall relative to the footwall (the shortening rate). The horizontal shortening rates for the thrust faults in this study suggest that the section of the Denali fault between the restraining bend apices is translating in the thrust fault transport direction (northwestward) at a rate on the order of 0.5 mm/yr (Figure 5.2)

There is still about 2.9 mm/yr of slip not accounted for. Where else could the lateral slip of the Denali fault be partitioned? We know that Mount McKinley is actively uplifting, and Fitzgerald et al. (1995) indicate a long-term exhumation rate of ~1 mm/yr. This leaves 1.9 mm/yr which 0.5 mm/yr can be used to accommodate faults east of apex, and alittle over 1 mm/yr can be used by the Peter Dome and other faults west of the apex. The active deformation to the west of the apex led to my assumption that the shortening rate would be higher along those faults.

4) How is the Mount McKinley restraining bend evolving?

Whether a restraining bend is stationary or migrating along a strike-slip fault has implications for how crustal material moves through the bend and how this deformation is accommodated structurally. There are no active strike-slip faults parallel to the Denali fault along the MMRB that separate the thrust fault sections to suggest a migrating bend. The only strike-slip fault of the foothills is the tear fault called Peters Dome fault 3 which is perpendicular to the Denali fault (Figure 4). Also there are no discrete offset geomorphic features to provide evidence for recent strike-slip displacement on the thrust faults, but the right stepping deformation front moving to the west. The migration of the apex of the bend to the southwest would need the progressive development of new traverse structures along the Denali fault to allow movement of the structure into new crustal material. The thrust faults are these structures allowing for translation of crust into the foreland to accommodate the transfer and migration of strain from the Denali fault to the west/northwest across the MMRB (Wakabayashi et al., 2004).

The combination of the northwestward uplift of the hanging wall of the thrust faults with the southwestward motion of the crust south of the Denali fault produces the southwest migration of the eastern apex of the restraining bend (Figure 5.1).To visualize the migrating apex, I see the apex as a rolling hinge being accommodated by the thrust faults moving crust to the northwest and the Denali fault pushing from behind. The transport direction and rate of the thrust faults, with the southwest movement of crust along the Denali fault, control the rate at which

the apex of the MMRB migrates. Although, the migration rate is unknown without more slip rate estimates of the other faults near the eastern apex.

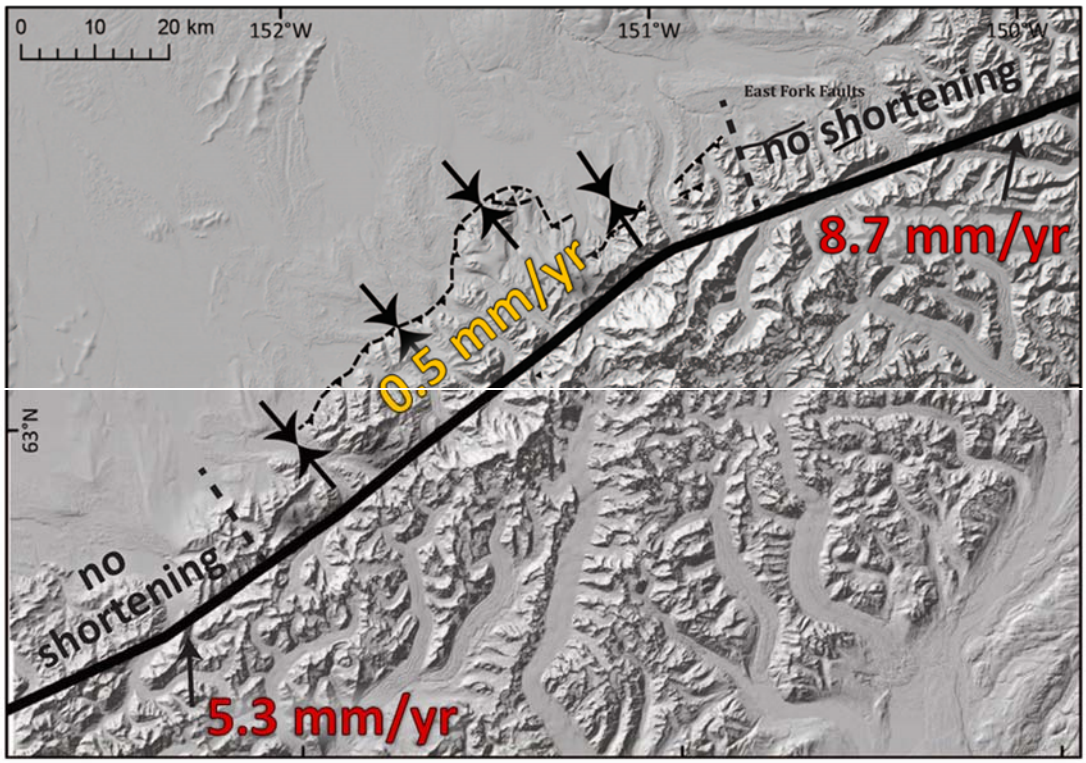

Figure 5.2: Bend migration. The Mount McKinley restraining bend of the Denali fault has a clear spatial relationship of active thrust faults along the restraining bend. The black inward-pointing arrows illustrate the region of Denali fault undergoing normal shortening at and to the west of the apex from east of the apex where there is no Neotectonic evidence for late Quaternary shortening.

Using completed core descriptions and photographs of split core sections from the three vibra-core transects, stratigraphic diagrams were produced for each transect. With the acquisition of precise GPS leveling data, the diagrams were scaled vertically (with respect to NAVD 88), as well as horizontally in order to accurately represent fault-induced deformation and offsets of major stratigraphic boundaries. These diagrams were also used to identify and select appropriate stations/depths for ^{14}C subsampling. Additionally, detailed core descriptions and photographs allowed for measurements of thicknesses of defined lithostratigraphic units and across-fault comparisons of these values.

CHAPTER SIX: CONCLUSIONS

Restraining bends are a common structure for producing enhanced shortening where bends occur in otherwise continuous strike-slip faults (Crowell, 1974; Biddle and Christie-Blick, 1985). MMRB formed in an intracontinental setting in central Alaska inside the dominant strike-slip fault system that is the Denali fault. The Denali fault system is formed on a past suture zone that concentrates the far-field stress of the southern plate boundary. The subduction plate boundary is still a main driving component of central Alaska's deformation today, but our research has shown that the local geology controls how that strain is concentrated and dispersed across the Mount McKinley restraining bend.

The MMRB structure and deformation has allowed for the tallest mountain in North America to grow within it. To achieve an exhumation of this magnitude to produce Mount McKinley, a typical restraining bend would have been long lived and fixed for an extended period of time. However, The MMRB is not a stationary feature of the Denali fault and the eastern apex of the retraining bend has migrated 10s of kilometers in relation to the East Fork faults area. In particular, this restraining bend is migrating to the southwest along the Denali fault, which is the same direction as the crust south of the Denali fault. The eastern apex through is moving at a slower rate, allowing for continuous rock uplift inside the restraining bend to achieve the tall, broad Alaska Range and Mount McKinley.

The Denali fault parallel thrust faults to the north of the bend are working to translate material into the foreland to accommodate the migration of the bend, since there is no evidence for strike-slip faults between the thrust fault sections parallel to the Denali fault. This allows for strain to migrate in right stepping thrust faults away from the Denali fault forming the northwest thrust pattern. Seismologic and neotectonic constraints suggest that the migration of the bend has led to the rotation of the maximum compressive stress axis. At most it has rotated 90 degrees from vertical east of the bend to horizontal and Denali fault-normal west of the bend. This allowed for south-side down normal slip motion on the East Fork faults. With shortening on the north side of the MMRB focused between the bend apices, it appears that the active deformation migration has progressively shut off the previous displacement of the East Fork faults or shortening to the east of the apex of the MMRB. There is a direct relationship between the deformation of the restraining bend and the seismicity of the Kantishna Cluster.

.

REFERENCES

Anderson E. M., 1951, The Dynamics of Faulting and Dyke Formation with Application to Britain: Oliver & Boyd, White Plains, N.Y., 206 p.

Balco, G. and Rovey II, C.W., 2008, An isochron method for comsogenic-nuclide dating of buried soils and sediments: American Journal of Science, v. 308, p. 1083-1114.

Balco, G. and Shuster, D. L., 2009, Al-26—Be-10—Ne-21 burial dating: Earth and Planetary Science Letters, p. 1-6.

Bayasgalan, A., Jackson, J., Ritz, J. and Carretier, S., 1999, Field examples of strike-slip fault terminations in Mongolia and their tectonic significance: Tectonics, v. 18, doi:10.1029/1999TC900007.

Bemis, S.P., Weldon, R., Carver, G., in review, Slip-partitioning along a continuously curved fault: Quaternary geologic controls on Denali fault system slip-partitioning, growth of the Alaska Range, and the tectonics of south-central Alaska: Pending acceptance with Lithosphere

Bemis, S.P., Carver, G.A., Koehler, R.D., 2012, The Quaternary thrust system of the northern Alaska Range: Geosphere, p. 1-11: doi:10.1130/GES00695.1

Bemis, S.P., and Wallace, W.K., 2007, Neotectonic framework of the north-central Alaska Range foothills, in Ridgway, K.D., Trop, J.M., Glen, J.M.G., and O'Neill, J.M. eds., Tectonic Growth of a Collisional Continental Margin: Crustal Evolution of Southern Alaska: Geological Society of America Special Paper 431, p. 549-572.

Biddle, K. T. and Christie-Blick, N. (eds), 1985, Strikeslip Deformation, Basin Formation, and Sedimentation: SEPM Special Publications, v. 37, 386 p.

Briner and Kaufman, 2008, Late Pleistocene mountain glaciation in Alaska: key chronologies: Journal of Quaternary Science, v. 23, p. 659-670.

Bronk-Ramsey, C., 2001, Development of the radiocarbon calibration program OxCal: Radiocarbon, v. 43, no. 2A, p. 355-363.

Burris, L.A., 2007, Seismicity and stresses in the Kantishna Seismic Cluster, Central Alaska: M.S. Thesis, University of Alaska Fairbanks, 87 p.

Csejtey, B., Jr., Mullen, M.W., Cox, D.P., and Stricker, G.D., 1992, Geology and geochronology of the Healy quadrangle, south-central Alaska: U.S. Geological Survey Miscellaneous Investigation Map I-1961.

Cooke, M.L., Schottenfeld, M.T., and Buchanan, S.W., 2013, Evolution of fault efficiency at restraining bends within wet kaolin analog experiments: Journal of Structural Geology, v. 51, p. 180-192, doi: http://dx.doi.org/10.1016/j.jsg.2013.01.010.

Cowgill, E., Yin, A., Arrowsmith, J. R., Feng, W. X., and Zhang, S. H., 2004a, The Akato Tagh bend along the Altyn Tagh fault, northwest Tibet 1: Smoothing by vertical-axis rotation and the effect of topographic stresses on bend-flanking faults: Geology Society of America Bulletin, v. 116, no.11-12, p.1423-1442.

Crowell, J. C., 1974, Origin of late Cenozoic basins in southern California, In: Dickinson, W. R., (ed.) Tectonics and Sedimentation: SEPM Special Publications, v. 22, 190-204 p.

Cronin, V., (2010), A Primer on Focal Mechanism Solutions for Geologists: Baylor University, p. 1-14.

Cunningham, W. D. and Mann, P., 2007, Tectonics of Strike-Slip Restraining and Releasing Bends, in Cunningham, W. D. and Mann, P. eds., Tectonics of Strike-Slip Restraining and Releasing Bends: Geological Society, London, Special Publications, v. 290, p. 1–12, doi: 10.1144/SP290.1.

Cunningham, W.D., 2007, Structural and topographic characteristics of restraining bend mountain ranges of the Altai, Gobi Altai, and easternmost Tien Shan, in Cunningham, W. D. and Mann, P. eds., Tectonics of Strike-Slip Restraining and Releasing Bends: Geological Society, London, Special Publications 2007, v. 290, p219 – 237, doi: 10.1144/SP290.7.

Davis, K, Burbank, D.W., Fisher, D., Wallace, S., and Nobes, D., 2005, Thrust-fault growth and segment linkage in the active Ostler fault zone New Zealand, Journal of Structural Geology, v. 27, p. 1528-1546.

Dewey, J.F., 1977, Suture zone complexities: A review: Tectonophysics, v. 40, p. 53-67.

Dortch, J. M., 2006, Defining the Timing of Glaciation in the Central Alaska Range: Master's thesis, University of Cincinnati, 82 pp.

Dortch, J.M., Owen, L.A., Caffee, M.W., and Brease, P., 2009, Late Quaternary glaciation and equilibrium line altitude variations of the McKinley River region, central Alaska Range: BOR, 14 p., doi: 10.1111/j.1502-3885.2009.00121.

Dortch, J.M., Owen, L.A., Caffee, M.W., LI, D., and Lowell, T.V., 2010, Beryllium-10 surface exposure dating of glacial successions in the Central Alaska Range: Jounral of Quaternary Science, v. 25, p. 1259-1269.

Eberhart-Phillips, D., Christensen, D.H., Brocher, T.M., Hansen, R., Ruppert, N.A., Haeussler, P.J., and Abers, G.A., 2006, Imaging the transition from Aleutian subduction to Yakutat collision in central Alaska, with local earthquakes and active source data: Journal of Geophysical Research, v. 111, p. B11303.

Ferris, A., Abers, G. A., Christensen, D.H., and Veenstra, E., 2003, High resolution image of the subducted Pacific (?) plate beneath central Alaska, 50-150km depth: Earth Planetary Science Letters, v. 214, p. 575-588.

Fitzgerald, P. G., S. M. Roeske, J. A.Benowitz, S. J. Riccio, S. E. Perry, and P. A.Armstrong, 2014, Alternating asymmetric topography of the Alaska range along the strike-slip Denali fault: Strain partitioning and lithospheric control across a terrane suture zone: Tectonics, v. 33, 15 p., doi:10.1002/2013TC003432.

Freymueller, J.T., Woodard, H., Cohen, S., Cross, R., Elliott, J., Larsen, C., Hreinsdottir, S., Zweck, C., 2008, Active deformation processes in Alaska, based on 15 years of GPS measurements, in Active Tectonics and Seismic Potential of Alaska: AGU Geophysical Monograph, v. 179, J.T. Freymueller, P.J. Haeussler, R. Wesson, and G. Ekstrom, eds., p. 1-42..

Gilbert, W. G., Ferrell, V. M., and Turner, D. L., 1976, The Teklanika Formation: a new Paleocene volcanic formation in the central Alaska Range: Alaska Division of Geological & Geophysical Surveys Geologic Report GR 0047, 16 p., 1 sheet, scale 1:63,360.

Granger, D. E. and Muzikar, P. F., 2001, Dating sediment burial with in situ-produced cosmogenic nuclides: theory, techniques, and limitations: Earth and Planetary Science Letters, v. 188, p. 269-281.

Haeussler, P.J., 2008, An Overview of the Neotectonics of Interior Alaska: Far-Field Deformation From the Yakutat Microplate Collision, in Freymueller, J.T., Haeussler, P.J., Wesson, R.L., and Ekström, G. eds., Active Tectonics and Seismic Potential of Alaska: American Geophysical Union Geophysical Monograph Series 179, Washington, D.C, p. 83–108.

Haeussler, P.J., Matmon, A., Schwartz, D.P., Seitz, G., and Crone, A.J., 2012, The Denali fault and interior Alaska tectonics in mid- to late-Cenozoic time, Abstract T14A-04 presented at 2012 Fall Meeting, AGU, San Francisco, Calif., 3-7 Dec.

Harding, T. P., 1985, Seismic characteristics and identification of negative flower structures, positive flower structures, and positive structural inversion: Bulletin of the American Association of Petroleum Geologists 69, v. 4, p. 582-600.

Jadamec, M.A., Billen, M.I., and Roeske, S.M., 2013, Three-dimensional numerical models of flat slab subduction and the Denali fault driving deformation in south-central Alaska: Earth and Planetary Science Letters, v. 376, p. 29–42, doi: 10.1016/j.epsl.2013.06.009.

Koehler, R.D., Farrell, Rebecca-Ellen, Burns, P.A.C., and Combellick, R.A., 2012, Quaternary faults and folds in Alaska: A digital database, in Koehler, R.D., Quaternary Faults and Folds (QFF): Alaska Division of Geological & Geophysical Surveys Miscellaneous Publication 141, 31 p., 1 sheet, scale 1:3,700,000. doi:10.14509/23944

Labay, K.A. and Haeussler, P.J., 2007, 3D visualization of earthquake focal mechanisms using arcscene: U.S. Geological Survey, 17 p.

Legg, M.R., Goldfinger, C., Kamerling, M.J., Chaytor, J.D., Einstein, D.E., 2007, Morphology, structure and evolution of California Continental Borderland restraining bends, in Cunningham, W. D. and Mann, P. eds., Tectonics of Strike-Slip Restraining and Releasing Bends: Geological Society, London, Special Publications 2007, v. 290, p. 143-168, doi:10.1144/SP290.3

Little, T.A., 1990, Kinematics of wrench and divergent-wrench deformation along a central part of the Border Ranges fault system, northern Chugach Mountains, Alaska: Tectonics, v. 9, p. 585–611.

Peterson, D.W., 1961, Descriptive model classification of igneous rocks: Am. Geol. Inst. Data sheets, 23a-23c.

Mann, P., 2007, Global catalogue, classification and tectonic origins of restraining and releasing bends on active and ancient strike-slip fault systems, in Cunningham, W. D. and Mann, P. eds., Tectonics of Strike-Slip Restraining and Releasing Bends: Geological Society, London, Special Publications, v. 290, p. 13-142, doi: 10.1144/SP290.2.

Matmon, A., Briner, J.P., Carver, G., Bierman, P., and Finkel, R.C., 2010, Moraine chronosequence of the Donnelly Dome region, Alaska: Quaternary Research, v. 74, no. 1, p. 63–72, doi: 10.1016/j.yqres.2010.04.007.

Matmon, A., Schwartaz, D.P., Haeussler, P.J., Finkel, R., Lienkaemper, J.J., Stenner, H.D., and Dawson, T., 2006, Denali fault slip rates and Holocene-late Pleistocene kinematics of central Alaska: Geology, v. 34, no.8, p. 645-648.

Mériaux, A.S., Sieh, K., Finkel, R.C., Rubin, C.M., Taylor, M.H., Meltzner, A.J., and Ryerson, F.J., 2009, Kinematic behavior of southern Alaska constrained by westward decreasing postglacial slip rates on the Denali Faults, Alaska: Journal of Geophysical Research, v. 114, 19 p.

Muzikar, P.F., 2011, Geological constraints and 26Al- 10Be burial dating isochrones: Earth Surface Processes and Landforms, v. 36, p. 946-952.

Ratchkovski, N.A. and Hansen, R.A., 2002, New constraints on tectonics of interior Alaska: Earthquake locations, source mechanism, and stress regime: Bulletin of the Seismological Society of America, v. 92, p. 998-1014.

Reed, B.L., and Lanphere, M.A., 1974, Offset Plutons and History of Movement along the McKinley Segment of the Denali Fault System, Alaska: Geological Society of America, Bulletin, v. 85, no. 12, p. 1883-1892.

Reed, J.C., Jr., 1961, Geology of the Mount McKinley quadrangle, Alaska: U.S. Geological Survey Bulletin, v. 11, no. 08-A, 36 p., scale 1 :63,360

Reger, R.D., Stevens, D.S.P, Solie, D.N., 2012, Surficial-Geologic map, Alaska Highway corridor, Delta Junction to Dot Lake, Alaska: Alaska Division of Geological and Geophysical Surveys, Sheet 1 of 2.

Ridgway, K.D., Thoms, E.E., Layer, P 286 .W., Lesh, M.E., White, J.M., and Smith, S.V., 2007, Neogene transpressional foreland basin development on the north side of the central Alaska Range, Usibelli Group and Nenana Gravel, Tanana basin, in Ridgway, K.D., Trop, J.M., Glen, J.M.G., and O'Neill, J.M. eds., Tectonic Growth of a Collisional Continental Margin: Crustal Evolution of Southern Alaska: Geological Society of America Special Paper 431, p. 507–547.

Ridgway, K.D., Trop, J.M., Nokleberg, W.J., Davidson, C.M., and Eastham, K.R., 2002, Mesozoic and Cenozoic tectonics of the eastern and central Alaska Range: Progressive basin development and deformation in a suture zone: Geological Society of America Bulletin, v. 114, no. 12, p. 1480–1504.

Ruppert, N.A., Ridgway, K.D., Freymueller, J.T., Cross, R.S., and Hansen, R.A., 2008, Active Tectonics of Interior Alaska: Seismicity, GPS Geodesy, and Local Geomorphology, in Freymueller, J.T., Haeussler, P.J., Wesson, R., and Ekström, G. eds., Active Tectonics and Seismic Potential of Alaska: American Geophysical Union Geophysical Monograph Series 179, Washington, D.C, p. 109–133.

Sanderson, D. J., and Marchini, W. R. D., 1984, Transpression: Journal of Structural Geology: v. 6, no. 5, p. 449-458.

Sylvester, A. G., and R. R. Smith, 1976, Tectonic transpression and basement-controlled deformation in San Andreas fault zone, Salton trough, California: AAPG Bulletin, v. 60, p. 2081-2102.

Ten Brink, N. W. and Waythomas, C. F.,1985, Late Wisconsin glacial chronology of the North-Central Alaska Range: A regional synthesis and its implications for early human settlements: National Geographic Research, Report 19, p. 15–33.

Teyssier, C., Tikoff, B., and Markley, M., 1995, Oblique plate motion and continental tectonics: Geology, v. 23, no. 5, p. 447-450.

Trop, J.M. and Ridgway, K.D., 2007, Mesozoic and Cenozoic sedimentary basin development along the inboard and outboard margins of the Wrangellia composite terrane: in Tectonic Growth of a Collisional Continental Margin: Crustal Evolution of Southern Alaska: Geological Society of America Special Paper 431, p. 55-94, doi:10.1130/2007.2431(04).

Thompson et al., 2002, Late Quaternary slip rates across the central Tien Shan, Kyrgyzstan, central Asia: Journal of Geophysical Research, v. 107, 32 p.

Wahrhaftig, C., 1958, Quaternary geology of the Nenana River valley and adjacent parts of the Alaska Range: U.S. Geological Survey Professional Paper 293–A, 1–118 p.

Wakabayashi, J., Hengesh, J.V. and Sawyer, T. L., 2004, Four-dimensional transform fault processes: progressive evolution of step-overs and bends: Tectonophysics, v. 392, p. 279–301.

Wakabayashi, J., 2007, Stepovers that migrate with respect to affected deposits: field characteristics and speculation on some details of their evolution, in Cunningham, W. D. and Mann, P. eds., Tectonics of Strike-Slip Restraining and Releasing Bends: Geological Society, London, Special Publications, 290, p. 169- 188.

Wesnousky, S. G., 1988, Seismological and structural evolution of strike-slip faults: Letters to Nature, v. 335, p. 340–343.

Wilson, F.H., Dover, J.H., Bradley, D.C., Weber, F.R., Bundtzen, T.K., and Haeussler, P.J., Geologic Map of Central (Interior) Alaska: U.S. Geological Survey Open-File Report OF 98-133-A, Version 1.2, http://pubs.usgs.gov/of/1998/of98-133-a/

VITA

Corey Austin Burkett

Education

B.S. Geology (2012)
West Virginia University

Experience

Graduate Research Assistant
University of Kentucky Department of Earth & Environmental Sciences
Lexington, KY 40506

Graduate Teaching Assistant
University of Kentucky Department of Earth & Environmental Sciences
Lexington, KY 40506